



# Timing and extent of Quaternary glaciations in the Tianger Range, eastern Tian Shan, China, investigated using $^{10}\text{Be}$ surface exposure dating



Yingkui Li <sup>a,\*</sup>, Gengnian Liu <sup>b</sup>, Yixin Chen <sup>b</sup>, Yanan Li <sup>a</sup>, Jon Harbor <sup>c,d</sup>, Arjen P. Stroeven <sup>d</sup>, Marc Caffee <sup>e</sup>, Mei Zhang <sup>b</sup>, Chuanchuan Li <sup>b</sup>, Zhijiu Cui <sup>b</sup>

<sup>a</sup> Department of Geography, University of Tennessee, Knoxville, TN 37996, USA

<sup>b</sup> College of Urban and Environmental Sciences, Peking University, Beijing 100871, China

<sup>c</sup> Department of Earth, Atmospheric, and Planetary Sciences, Purdue University, West Lafayette, IN 47907, USA

<sup>d</sup> Bolin Centre for Climate Research, Department of Physical Geography and Quaternary Geology, Stockholm University, S-106 91 Stockholm, Sweden

<sup>e</sup> Department of Physics, Purdue Rare Isotope Measurement Laboratory, Purdue University, West Lafayette, IN 47907, USA

## ARTICLE INFO

### Article history:

Received 3 December 2013

Received in revised form

13 May 2014

Accepted 15 May 2014

Available online

### Keywords:

Cosmogenic nuclides

Glacial chronology

Quaternary glaciations

Tian Shan

Central Asia

## ABSTRACT

Reconstructing glacial chronologies with consistent methods is critical for efforts to examine the timing and pattern of past climate change. Cosmogenic  $^{10}\text{Be}$  surface exposure dating has been widely used to constrain the timing of glacial events on the Tibetan Plateau and in Central Asia. However, few such studies have been conducted in the Chinese Tian Shan and available  $^{10}\text{Be}$  ages from this region have only provided evidence for glacial events during the global Last Glacial Maximum (gLGM) and Lateglacial. Here, we present 45  $^{10}\text{Be}$  surface exposure ages from glacial landforms in the Ala and Daxi valleys, two formerly glaciated valleys draining the Tianger Range, eastern Tian Shan. Combined with previously published  $^{10}\text{Be}$  surface exposure ages from the Daxi Valley in the source area of the Urumqi River, the new ages record five major glacial events during Marine Oxygen Isotope Stages (MIS) 6 or older, 4, 3, 2, and 1 (during the Little Ice Age, LIA). Landforms from glacial events since MIS 2 are found on the northern slope of the Tianger Range (Daxi Valley), whereas evidence for the older glacial events is only preserved on its southern slope (Ala Valley). This disparity may be caused by different preservation- and micro-climatic conditions on the northern and southern slopes of this mountain range, due to differences in gradient and aspect. The LIA glacial advances are apparently the only Holocene glacial event recorded in this area. Earlier Holocene glacial events were probably so restricted in extent that they were destroyed by subsequent LIA advances.

© 2014 Elsevier Ltd. All rights reserved.

## 1. Introduction

Mountain glaciers are sensitive to climate change, especially in regions located within the confluence of different climate systems (Ehlers and Gibbard, 2007; Thackray et al., 2008). Central Asia, in particular, is controlled by the interactions of the westerlies, the Siberian High, and potentially the Asian monsoon (Benn and Owen, 1998). Glaciers develop in its highlands, such as the Tian Shan, Altai, and Pamir, in response to temporal variations in the dominance of precipitation systems from the Atlantic Ocean, from closed drainage-basin sources such as the Aral, Black, and Caspian seas,

and from the Arctic Ocean (Benn and Owen, 1998; Kreutz et al., 2001; Olivier et al., 2003; Aizen et al., 2004, 2005; Henderson et al., 2006). Each of these systems might produce a distinctive pattern of glaciation within a region. These glaciation patterns will likely be complicated and reconstructing the timing and extent of past glacial variations is a critical element in achieving a comprehensive understanding of the impacts of these interacting climate systems.

Although some paleo-glacial reconstructions in Central Asia have been conducted (e.g. Yi et al., 2002; Abramowski et al., 2006; Zhao et al., 2006, 2009, 2010; Seong et al., 2007; Koppes et al., 2008; Kong et al., 2009; Li et al., 2011; Röhringer et al., 2012; Zech, 2012; Stroeven et al., 2013; Zech et al., 2013), this area has not been extensively studied. Dating glacial landforms and deposits in arid environments like this is challenging because there is

\* Corresponding author.

E-mail address: [yli32@utk.edu](mailto:yli32@utk.edu) (Y. Li).

usually a paucity of organic matter for radiocarbon dating in glacial deposits and landforms, and the timescale of radiocarbon dating (<50 ka) is insufficient to provide more than minimum-limiting ages for much older glacial events (Balco, 2011). Cosmogenic nuclide surface exposure dating (mostly  $^{10}\text{Be}$ ) has been and continues to be used to improve glacial chronologies in the Central Asian highlands (e.g. Abramowski et al., 2006; Seong et al., 2007; Koppes et al., 2008; Kong et al., 2009; Li et al., 2011; Röhringer et al., 2012; Zech, 2012; Zech et al., 2013). Except for a few sites from the eastern Tian Shan (Kong et al., 2009; Li et al., 2011), most  $^{10}\text{Be}$  surface exposure dating studies of glacial landforms have been conducted in the western Tian Shan and in the Pamir (Abramowski et al., 2006; Seong et al., 2007; Koppes et al., 2008; Röhringer et al., 2012; Zech, 2012; Zech et al., 2013).

The source area of the Urumqi River in the Tianger Range of the eastern Tian Shan is one of the few sites where glacial landforms and deposits have been dated using  $^{10}\text{Be}$  surface exposure dating (Kong et al., 2009; Li et al., 2011). It is also one of the most intensively studied field areas in the world for glacial geomorphology because of its spectacular landforms and the presence of a research station of the Chinese Academy of Sciences (Tianshan Glaciological Station) in the Daxi Valley since 1959. In addition to  $^{10}\text{Be}$  surface exposure dating, other techniques used to date glacial landforms and deposits in this valley include radiocarbon ( $^{14}\text{C}$ ), lichenometry, thermoluminescence, and electron spin resonance (ESR) (Wang, 1981; Zheng and Zhang, 1983; Chen, 1989; Li, 1995; Yi et al., 2002, 2004; Zhao et al., 2006). However, few studies have been conducted in adjacent valleys on the northern slope of the Tianger Range, and there is no glacial chronology established from the southern side of the mountain range.

Our primary focus was on establishing a glacial chronology in the Ala Valley, a major formerly-glaciated valley on the southern side of the Tianger Range using cosmogenic  $^{10}\text{Be}$  surface exposure dating. We also collected samples from a suspected Little Ice Age (LIA) moraine in the Daxi Valley for exposure age determination. These measurements, together with published  $^{10}\text{Be}$  exposure ages in this area, allow for a comparison of the timing and extent of Quaternary glaciations on both sides of the Tianger Range. We also compare the composite  $^{10}\text{Be}$ -derived glacial chronology with published ESR ages from this area to evaluate the performance of ESR in dating glacial deposits.

## 2. Geomorphologic setting and previous work

The Tian Shan, known as the “Water Tower of Central Asia” (Sorg et al., 2012) because of an abundance of glaciers, is a WSW–ENE trending ~2500 km long arc of mountains extending from the western boundary of Kyrgyzstan, across most of the Xinjiang

Uyghur Autonomous Region, China, almost to the Mongolian border (Fig. 1). It is one of the driest regions in the world. The orographic effect of this mountain range leads to a pronounced gradient in precipitation from northwest (annual precipitation of 1500–2000 mm) to southeast (~100 mm) (Sorg et al., 2012). The geomorphological imprint of Quaternary glaciations varies along the length of the Tian Shan and mirrors the distribution of the highest peaks (Stroeven et al., 2013). The climate of the Tian Shan is presently dominated by the westerlies and the Siberian High (Benn and Owen, 1998). The shifting dominance of these two circulation systems are expected to have played a key role in driving the timing and extent of Quaternary glaciations in this area.

The Tian Shan consists of several smaller mountain ranges including the Tianger Range in the eastern Tian Shan. The highest peak of the Tianger Range is Tianger Peak II (43.111°N, 86.798°E; Fig. 2) at ~4486 m above sea level (m a.s.l.). Modern glaciers around this peak occur mainly within the north-facing valleys and cirques, and are limited to cirque glaciers, hanging glaciers, and small valley glaciers. Abundant glacial landforms, erratics, and deposits are distributed along major valleys >10 km downstream from modern glaciers or from headwalls in ice-free valleys (Fig. 2).

The source area of the Urumqi River is located in the Daxi Valley on the northern slope of the Tianger Range (Fig. 2). This area is particularly well known in glacial geomorphology because of the presence of double (U-in-U) troughs in formerly glaciated valleys (Cui, 1981; Li et al., 2001a,b). Five groups of moraines have been identified in the Daxi Valley. Detailed description of these moraines and other related glacial landforms can be found in Zhao et al. (2006) and Li et al. (2011). Although glacial landforms and deposits within this valley have been dated using multiple techniques, there is still some controversy about their ages. This controversy arises primarily because of differences between  $^{10}\text{Be}$  and ESR ages:  $^{10}\text{Be}$  ages date only to the global Last Glacial Maximum (gLGM), whereas ESR ages from the same landforms are significantly older (ranging from 27 to 184 ka, Yi et al., 2002; Zhao et al., 2006).

The Ala Valley is a major south-facing, formerly-glaciated valley on the southern slope of the Tianger Range (Fig. 2). Most glaciers within this valley have disappeared and only a few small glaciers remain, perched within shaded north-facing cirques in valley heads. We investigated glacial landforms/deposits distributed from the valley head of the west branch of the Ala Valley (Arexigongjin (AR) Valley, around 3800 m a.s.l.) to the confluence between the Ala Valley and the Dundesala (DDSL) Valley around 2900 m a.s.l. (Fig. 2). Several groups of moraines remain well preserved in this >20 km long valley section.

There is a set of fresh-looking lateral-terminal moraines a few hundred meters away from the terminus of the modern glacier near

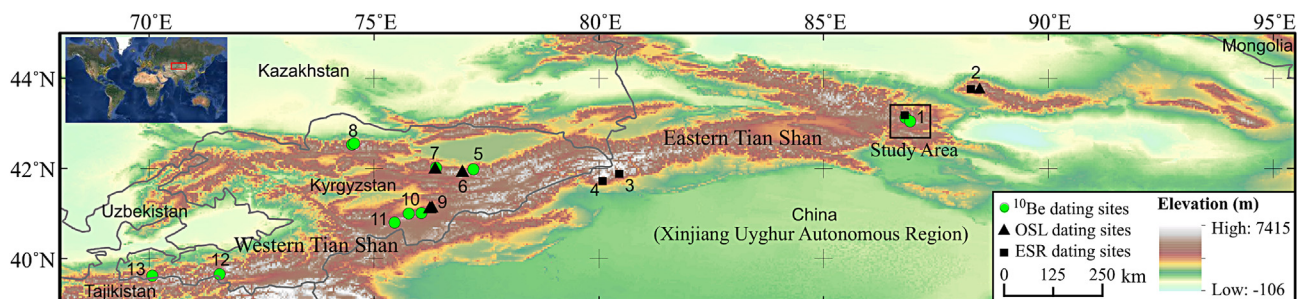


**Fig. 1.** Relief map of the Tian Shan illustrating available  $^{10}\text{Be}$ , OSL, and ESR dating studies across the Tian Shan. (1) Daxi (Yi et al., 2002; Zhao et al., 2006; Kong et al., 2009; Li et al., 2011; this paper) and Ala (this paper) valleys, Tianger Range; (2) Heigou and Gubanbogada valleys, Bogeda Range (Zhao et al., 2012); (3) Muzart Valley (Zhao et al., 2010); (4) Ateoyinake Valley (Zhao et al., 2009); (5) Gulbel Pass, Terskey Ala Tau Range (Koppes et al., 2008); (6) Temir-Kanat area, Terskey Ala Tau Range (Narama et al., 2009); (7) Ala Bash Basin (Koppes et al., 2008) and Turasu Valley (Narama et al., 2007), Terskey Ala Tau Range; (8) Ala Archa and Chor Kyrchak valleys, Kyrgyz Front Range (Koppes et al., 2008); (9) Chong-Tör and Sary-Tal valleys, At Bashi Range (Narama et al., 2009); (10) Djo Bog Gulsh and Terekçu valleys, At Bashi Range (Koppes et al., 2008); (11) Kitschi-Kurumdu Valley, At Bashi Range (Zech, 2012); (12) Koksü Valley, Alay Range (Abramowski et al., 2006); and (13) Aksu Valley, Turkestan Range (Abramowski et al., 2006).

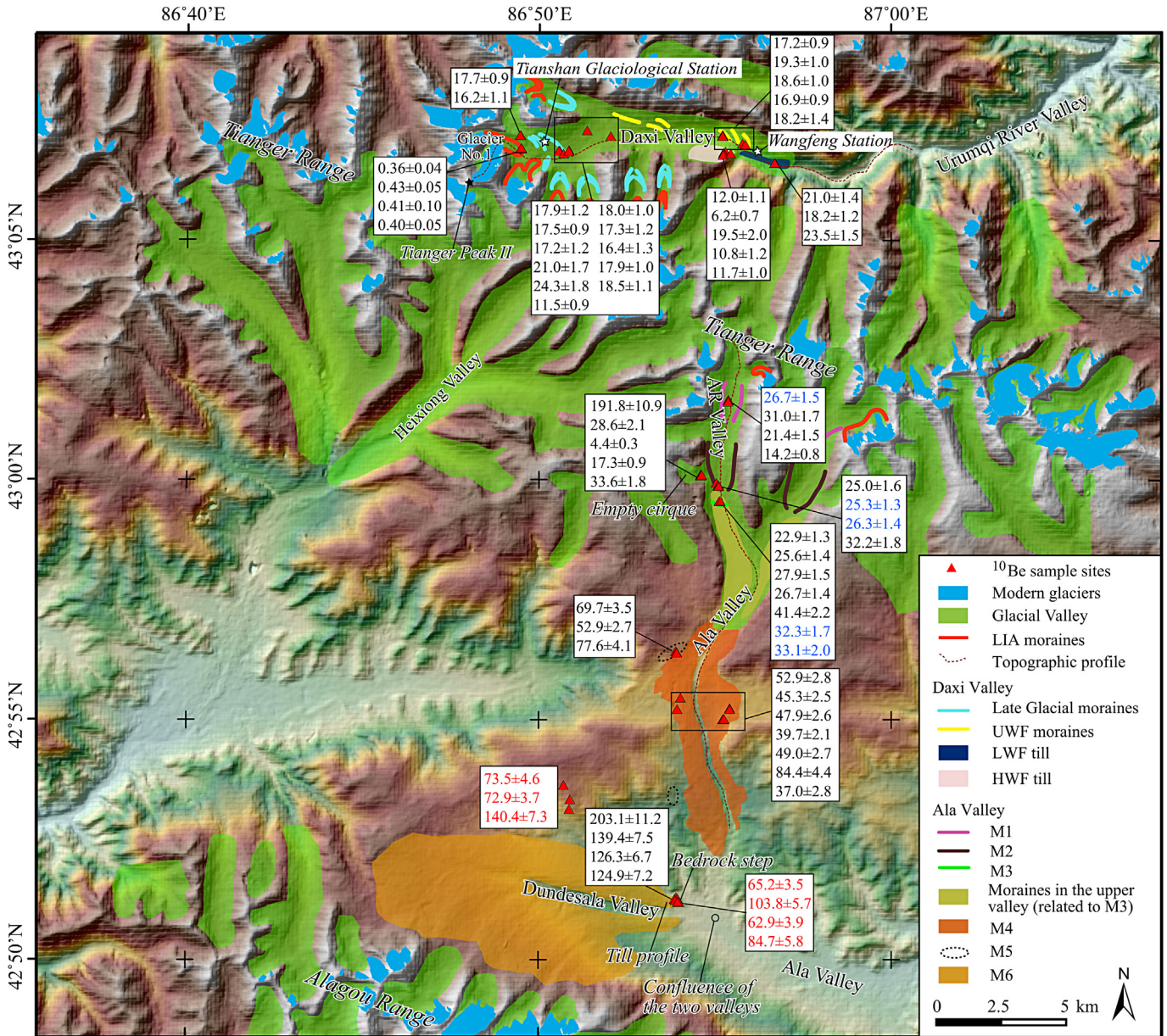


**Fig. 2.** Shaded relief map of the Tianger Range area, eastern Tian Shan, with detailed mapping of glacial landforms for the two formerly glaciated valleys of the northern (Daxi Valley) and southern (Ala Valley) slopes. This map also illustrates <sup>10</sup>Be exposure ages (in ka) from moraines and other glacial landforms in these two valleys (including data from Kong et al. (2009) and Li et al. (2011)). The ages in black are from boulder-, in red are from bedrock-, and in blue are from pebble samples. Black boxes indicate groups of <sup>10</sup>Be ages scattered within a relatively large area. Modern glaciers were delineated from Google Earth images of 2010. All previously published ages are re-calculated using CRONUS Earth 2.2 calculator (Balco et al., 2008) under the assumption of zero erosion (reported ages are based on the scaling model of Lal (1991)/Stone (2000) with time-dependent production rate; Tables 2, 4). The characteristics of the two topographic profiles along these two valleys are illustrated in Fig. 6A. AR: Arexigongjin. (For interpretation of the references to color in this figure legend, the reader is referred to the web version of this article.)

the head of the AR Valley. We were not able to visit these moraines due to bad weather. Google Earth high-resolution imagery indicates that these moraines have similar characteristics to the fresh moraines in front of Glacier No. 1 in the Daxi Valley (Fig. 2). These moraines in front of Glacier No. 1 have been dated by lichenometry (Chen, 1989) and by AMS <sup>14</sup>C dating of inorganic carbonate coatings (Yi et al., 2004), indicating formation during the LIA.

The AR Valley and the upper section of the Ala Valley are filled with relatively flat hummocky moraines downstream from the fresh-looking moraines close to the modern glacier (Fig. 2), down to an elevation of about 3350 m a.s.l., which is 2–3 km downstream from the point where the two major branches of the Ala Valley join.

River incision is not apparent in this ~10 km long valley section. Some small recessional lateral or terminal moraines (<10 m in height, cf. Fig. 3A) occur in this section, indicating short stagnant phases of the glacier during retreat. Grasses and a thin soil layer cover the surfaces of these small moraines, and boulders on these moraines are slightly weathered and covered by lichens. This set of moraines indicates a glacial event to about 10 km down-valley from the modern glacier terminus. We investigated and sampled the ground moraine within an empty cirque half way down this valley section (EC), a lateral moraine (M1) about 3.0 km upstream from the empty cirque and about 1.5 km downstream from the LIA moraines, a lateral-terminal moraine close to the empty cirque

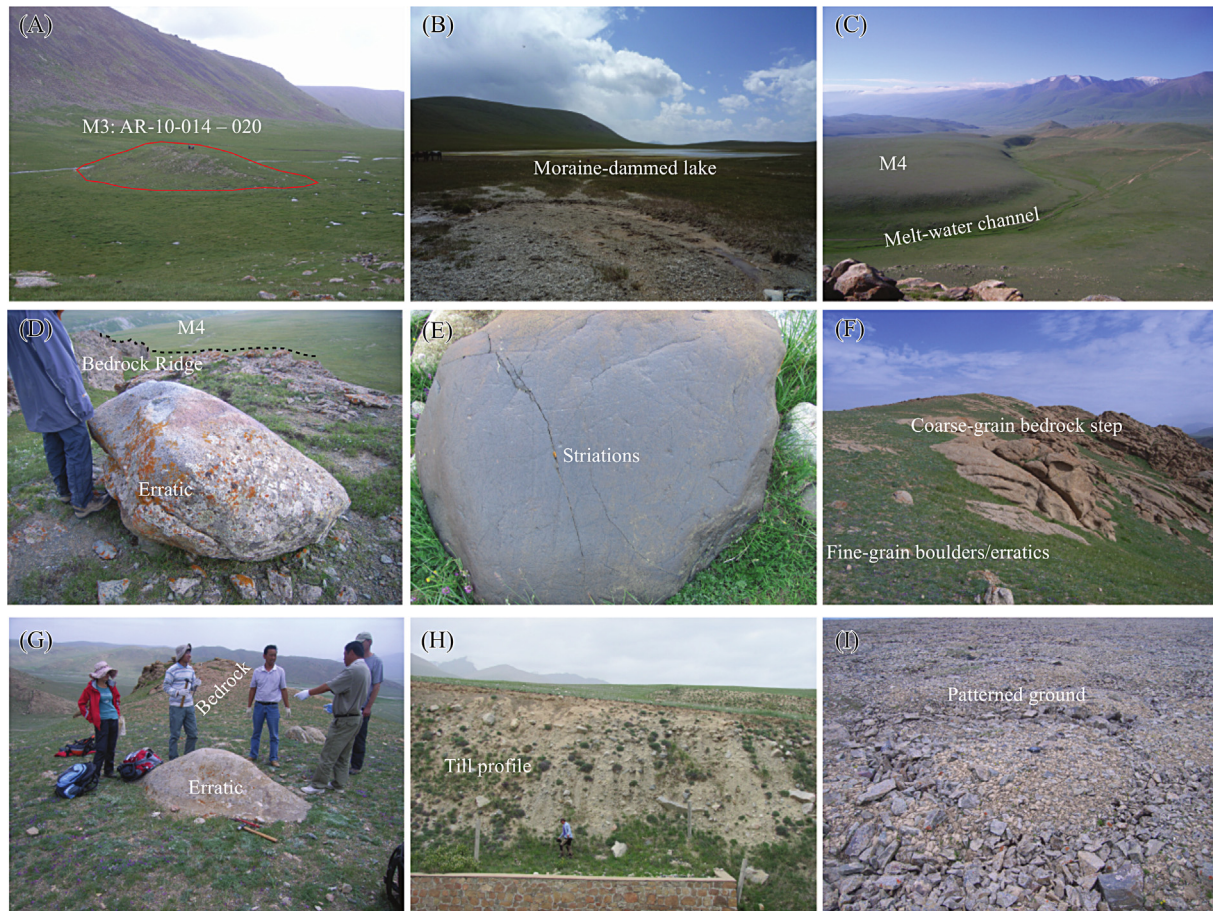


**Fig. 3.** Representative field sites in the Ala Valley. (A) A small end moraine (M3) in the valley; (B) A moraine-dammed lake behind M4; (C) The terminal moraine of M4 with a melt-water channel in the front of the moraine; (D) Boulder/erratic (M5) on top of bedrock, about 100 m higher than M4; (E) Faceted and striated clast found outside of M4 around 2950 m a.s.l.; (F) Bedrock step at the confluence of the Ala and Dundesala valleys; (G) Same location as (F), showing different lithology of boulders/erratic (M6) on the bedrock step; (H) A till profile (M6) in a railway cut; (I) Patterned ground on top of a relatively flat summit surface (3940 m a.s.l.).

(M2), and a terminal moraine about 1.0 km downstream from the empty cirque (M3, Fig. 2).

A spectacular set of lateral-end moraines (M4) occurs on both sides of the main Ala Valley before the confluence with the Dundesala Valley, from ~3350 m to ~2950 m a.s.l. (Fig. 2). Stream cuts in the valley bottom expose till profiles and this moraine set terminates with many small ridges (hummocky moraine). The M4 glacier and the moraines it deposited dammed tributaries from both sides of the valley, forming moraine-dammed lakes (Fig. 3B). A series of melt-water channels cuts through the lateral and terminal moraines (Fig. 3C), indicating discrete positions of the ice margin during retreat. These moraines, which are covered by grasses and soil with a few large weathered boulders exposed on top, indicate a glacial event >20 km down-valley from the modern glacier terminus. We investigated and sampled lateral moraines on both sides of the valley where moraine-dammed lakes occur.

We found boulders and till remnants (M5, Fig. 3D) scattered on bedrock ridges and tors at ~3400 m a.s.l., approximately 100 m above the M4 moraine set. The lithology of the boulders on M5 is similar to the boulders on M4, but the boulder surfaces on M5 are more weathered than those on M4. Beyond the furthest extent of M4, at ~2950 m a.s.l., we also discovered erratics with glacial striations and polished surfaces (Fig. 3E) scattered on bedrock ridges. These erratics may correspond to an ice extent which simultaneously deposited the M5 boulders and tills at ~3400 m a.s.l. above M4. The appearance of these boulders/erratics and till remnants

indicates a significantly older and more extensive glacial event in this valley than during M4.

A bedrock step covered by a thin layer of glacial deposits (M6; Fig. 2) occurs at the confluence between the Ala and Dundesala valleys. The bedrock consists predominantly of coarse-grained highly-weathered granite (Fig. 3F). It is removed easily without a hammer and chisel. In contrast, boulders scattered on top of the bedrock consist mainly of fine-grained granite. The surfaces of the boulders were weathered, but extremely hard to sample with chisels for  $^{10}\text{Be}$  surface exposure dating (Fig. 3G). A >10 m-high till profile is exposed in a railway cut behind the bedrock step (Fig. 3H). Based on position, this till was most likely deposited by ice from the Dundesala Valley. However, the lithology of the boulders is similar to that of M1–M5 in the Ala Valley and glacial deposits from both valleys would have been combined when the glaciers merged and advanced to this position. Downstream from this bedrock step, fluvial erosion has been extensive. If glacial deposits existed downstream from the bedrock step, then they were most likely eroded by fluvial erosion.

Most glacial valleys on the southern slope of the Tianger Range cut into a relatively flat and smooth summit surface (Fig. 2). Periglacial landforms, including patterned ground, blockfields, and tors, decorate these summit ridges and interfluvies (Fig. 3I). A few large boulders of uncertain origin occur on these ridges and divides, indicating that, if they are erratics, this area may have been covered by a large ice cap or ice field that was likely cold-based over the summits.

### 3. Material and methods

We used Google Earth high-resolution imagery and a 90 m-resolution digital elevation model (DEM) of the Shuttle Radar Topography Mission (SRTM, <http://srtm.csi.cgiar.org>) to identify and map glacial features on the northern and southern slopes of the Tianger Range, focusing on the Daxi Valley and the Ala Valley (Fig. 2). The glacial features identified from Google Earth and SRTM DEM were sampled after field observations verified that cosmogenic nuclide analyses might yield meaningful exposure ages. Approximately 0.5–1.0 kg of rock of the upper 0.5–5.0 cm was collected from the flat top of each target boulder. Boulders on tops of moraines were selected to minimize the potential impact of shielding (by snow and sediment) and toppling on cosmogenic nuclide concentrations. Most samples were taken from large (>1 m) granite and gneiss boulders (Table 1). Several samples consisting of pebbles from moraine surfaces were collected to evaluate moraine surface stability by comparing the ages of boulders and pebbles (Briner, 2009; Heyman et al., 2011a). To evaluate bedrock erosion rates we also collected bedrock samples from the rock step associated with M6 till and tors on top of interfluve ridges (Fig. 2, Table 1). A GPS unit was used to record sample locations and altitudes. Shielding from surrounding mountain slopes and dip angles of the sample sites were measured to determine the topographic shielding factor. In total, we collected twenty-nine boulder-, five pebble-, and seven bedrock samples from the Ala Valley (Table 1). We also collected four samples from the outmost fresh moraine in front of Glacier No. 1 in the Daxi Valley (Fig. 2, Table 1) to provide an  $^{10}\text{Be}$  age constraint of this moraine that has been dated to the LIA by lichenometry (Chen, 1989) and AMS  $^{14}\text{C}$  (Yi et al., 2004).

Most samples were prepared in the cosmogenic nuclide sample preparation laboratory of the Institute of Tibetan Plateau Research, Chinese Academy of Sciences. Four samples collected from the fresh moraine in front of Glacier No. 1 were prepared in the Purdue Rare Isotope Measurement Laboratory (PRIME Lab) at Purdue University. Quartz was separated for each sample using modified procedures based on Kohl and Nishiizumi (1992). The quartz was then dissolved in HF and  $\text{HNO}_3$  and spiked with 0.3–0.6 mg  $^9\text{Be}$  carrier. AMS measurements were carried out at PRIME Lab based on the revised ICN standard (Nishiizumi et al., 2007). Measured  $^{10}\text{Be}/^9\text{Be}$  ratios were corrected by full chemistry procedural blanks ( $5.4 \pm 1.3 \times 10^{-15}$  for samples from the Ala Valley and  $12.0 \pm 3.0 \times 10^{-15}$  for samples from Glacier No. 1) and converted to  $^{10}\text{Be}$  concentrations.<sup>1</sup>

We calculated minimum  $^{10}\text{Be}$  exposure ages (Table 2) using CRONUS Earth 2.2 calculator (Balco et al., 2008) based on different scaling models and the assumption of zero erosion (Lal, 1991). We used the reference  $^{10}\text{Be}$  production rate of the calibration dataset from NE North America (NENA) (Balco et al., 2009) in the calculation because most estimates of  $^{10}\text{Be}$  production rates published since Balco et al. (2009), with broad geographic coverage, generally agree within uncertainties with those values (e.g. Putnam et al., 2010; Kaplan et al., 2011). For samples collected from bedrock surfaces, we also calculated the maximum erosion rates of the surfaces using the CRONUS Earth 2.2 calculator with different scaling models based on the assumption of long-term continuous exposure of the bedrock surface (Lal, 1991; Table 3). The topographic shielding factor was calculated using a python tool and the SRTM DEM with designated  $5^\circ$  intervals in both azimuth and elevation angles (Li, 2013). Comparing with the field-derived topographic shielding factors, Li (2013) demonstrated that the

model-derived topographic shielding factors using these intervals yielded consistent values. A sample thickness correction was determined using measured sample thickness and a rock density of  $2.7 \text{ g/cm}^3$ . We neglected the shielding from snow or vegetation cover in the calculation because it is likely minor due to the dry climatic condition and the scarce vegetation cover.

In the discussion we focus on ages calculated using the time-dependent scaling model of Lal (1991)/Stone (2000). To ensure valid comparisons with previously published data across the Tian Shan (Abramowski et al., 2006; Koppes et al., 2008; Kong et al., 2009; Li et al., 2011; Zech, 2012), we also recalculated those datasets using the same method (Table 4). The exposure ages from a moraine may be scattered due to several potential reasons/processes (Hallet and Putkonen, 1994; Putkonen and Swanson, 2003; Briner et al., 2005; Applegate et al., 2010; Balco, 2011; Heyman et al., 2011b): (1) uncertainties in the sample preparation and measurement; (2) nuclide inheritance caused by the exposure of a sample prior to glacial entrainment and deposition; (3) incomplete exposure caused by partial shielding as a result of post-glacial moraine degradation and exhumation. A spread of moraine exposure ages may also correspond to the duration of the standstill that built the moraine. Because a glacier acts as a conveyor belt transporting sediment to the moraine, in some cases the oldest ages could reflect the period post-dating glacial advance to the maximum position and the youngest ages pre-dating the onset of glacial retreat from the moraine. To better interpret surface exposure ages, we plotted probability density functions of all  $^{10}\text{Be}$  ages for each moraine to detect potential young/old outliers and to identify clusters in the ages (Fig. 4). After removing outliers by visually examining the probability density plot for each moraine (Fig. 4), we calculated reduced chi-squared statistics ( $\chi_R^2$ ) of the remaining cluster as described in Balco (2011) to determine if the scatter is due to measurement errors or geomorphic processes. If the scatter is simply due to measurement errors ( $\chi_R^2 \leq 1$ ), the weighted mean was used for the age of the moraine. Otherwise, we judged the scatter of the ages within the context of the relative geomorphic sequences and provided a range of ages for the corresponding moraine because there is not enough evidence to further judge if the scatter was caused by incomplete exposure (moraine degradation and exhumation), prior exposure, or other potential processes based on our available data. The formation age of the moraine is likely bracketed by the oldest and youngest ages of the assigned age range because it would be equal to or older than the youngest age (incomplete exposure possibility) and/or equal to or younger than the oldest age (prior exposure possibility).

We estimated the depressions of the equilibrium line altitudes (ELAs) relative to the ELAs of modern glaciers and the distances from the terminus of modern glaciers to examine the spatial pattern of the extent of Quaternary glaciations across the Tian Shan. Several methods have been introduced to estimate ELA based on mapped field evidence of former glacier extent, including the balance ratio (BR), the accumulation-area ratio (AAR), the maximum elevation of lateral moraines (MELM), the toe-to-headwall altitude ratio (THAR), the toe-to-summit altitude method (TSAM), and the cirque-floor altitude (Benn and Lehmkuhl, 2000). A recent study by Nie et al. (2014) suggested that the ELAs derived using different methods are moderately correlated in the Tianger Range, although differences exist due to the use of different parameters in each method. To avoid potential inconsistency among different methods, we employed a consistent method, TSAM, to estimate the ELA depressions of fifteen glacial valleys/sites along the Tian Shan where glacial chronologies have been constrained using  $^{10}\text{Be}$  or Optically-Stimulated Luminescence (OSL) dating (Table 5). TSAM determines the ELA by calculating the mean elevation between the highest peak within the glacier catchment and the elevation of the inferred

<sup>1</sup> Quartz weights,  $^9\text{Be}$  carrier masses, and AMS measured  $^{10}\text{Be}/^9\text{Be}$  ratios of these samples are listed in the online appendix.

**Table 1**  
Measured  $^{10}\text{Be}$  concentrations and parameters used in the surface exposure age calculation (Table 2) for samples from the Tianger Range, eastern Tian Shan, China.

Sample ID	Location	Moraine group, type (dimension)	Lithology	Latitude ( $^{\circ}\text{N}$ )	Longitude ( $^{\circ}\text{E}$ )	Elevation (m a.s.l.)	Thickness (cm)	Topographic shielding factor <sup>a</sup>	$^{10}\text{Be}$ concentration ( $10^5 \text{ atoms g}^{-1}$ ) <sup>b</sup>
AR-10-001	Ala Valley	Cirque, boulder (130 × 110 × 45 cm)	Gneiss	43.002	86.910	3660	2.0	0.9767	100.50 ± 2.45
AR-10-002	Ala Valley	Cirque, boulder (135 × 75 × 30 cm)	Granite	43.002	86.909	3662	4.0	0.9769	14.73 ± 0.77
AR-10-003	Ala Valley	Cirque, boulder (100 × 60 × 45 cm)	Granite	43.002	86.910	3659	3.0	0.9799	2.16 ± 0.10
AR-10-004	Ala Valley	Cirque, boulder (130 × 90 × 38 cm)	Granite	43.002	86.910	3651	5.0	0.9784	8.60 ± 0.14
AR-10-005	Ala Valley	Cirque, boulder (180 × 65 × 20 cm)	Granite	43.002	86.910	3658	4.0	0.9799	17.50 ± 0.37
AR-10-021	Ala Valley	M1, pebbles	Granite, quartzite	43.028	86.923	3618	1.5	0.9477	13.23 ± 0.38
AR-10-022	Ala Valley	M1, boulder (100 × 60 × 35 cm)	Granite	43.028	86.923	3617	3.0	0.9477	15.32 ± 0.38
AR-10-023	Ala Valley	M1, boulder (70 × 60 × 35 cm)	Granite	43.027	86.923	3616	3.0	0.9477	10.37 ± 0.50
AR-10-024	Ala Valley	M1, boulder (130 × 100 × 90 cm)	Granite	43.027	86.923	3613	3.0	0.9485	6.75 ± 0.21
AR-10-007	Ala Valley	M2, boulder (110 × 85 × 20 cm)	Gneiss	42.999	86.917	3522	5.0	0.9735	11.68 ± 0.51
AR-10-009	Ala Valley	M2, pebbles	Granite, gneiss, quartzite	42.998	86.918	3514	3.0	0.9750	12.01 ± 0.16
AR-10-010	Ala Valley	M2, pebbles	Granite, gneiss, quartzite	42.998	86.918	3501	3.0	0.9734	12.39 ± 0.30
AR-10-011	Ala Valley	M2, boulder (120 × 95 × 20 cm)	Granite	42.998	86.918	3509	5.0	0.9734	15.12 ± 0.37
AR-10-014	Ala Valley	M3, boulder (60 × 40 × 15 cm)	Granite	42.993	86.919	3489	5.0	0.9694	10.41 ± 0.31
AR-10-015	Ala Valley	M3, boulder (55 × 40 × 15 cm)	Granite	42.993	86.919	3480	2.0	0.9694	11.96 ± 0.30
AR-10-016	Ala Valley	M3, boulder (70 × 30 × 10 cm)	Granite	42.993	86.919	3489	5.0	0.9694	12.83 ± 0.32
AR-10-017	Ala Valley	M3, boulder (130 × 70 × 10 cm)	Granite	42.993	86.918	3487	5.0	0.9694	12.20 ± 0.28
AR-10-018	Ala Valley	M3, boulder (30 × 30 × 10 cm)	Granite	42.993	86.918	3479	3.0	0.9694	19.69 ± 0.39
AR-10-019	Ala Valley	M3, pebbles	Granite, quartzite	42.993	86.918	3477	2.0	0.9694	15.23 ± 0.29
AR-10-020	Ala Valley	M3, pebbles	Granite, quartzite	42.993	86.919	3487	3.0	0.9694	15.59 ± 0.52
ARL-10-001	Ala Valley	M4, boulder (180 × 135 × 40 cm)	Gneiss	42.921	86.924	3283	3.0	0.9991	23.07 ± 0.48
ARL-10-002	Ala Valley	M4, boulder (125 × 70 × 17 cm)	Gneiss	42.921	86.924	3278	3.0	0.9991	19.81 ± 0.51
ARL-10-003	Ala Valley	M4, boulder (70 × 60 × 10 cm)	Quartzite	42.917	86.920	3272	3.0	0.9989	20.86 ± 0.46
ARL-10-004	Ala Valley	M4, boulder (140 × 118 × 26 cm)	Gneiss	42.917	86.920	3274	3.0	0.9989	17.18 ± 0.39
ARL-10-005	Ala Valley	M4, boulder (75 × 70 × 30 cm)	Gneiss	42.917	86.921	3275	4.0	0.9989	21.16 ± 0.55
KXN-10-022	Ala Valley	M4, boulder (205 × 190 × 40 cm)	Gneiss	42.921	86.899	3256	1.0	0.9991	36.48 ± 0.57
KXN-10-024	Ala Valley	M4, boulder (210 × 120 × 60 cm)	Gneiss	42.925	86.900	3271	3.0	0.9994	15.95 ± 0.93
ARL-10-006	Ala Valley	M5, boulder (130 × 90 × 40 cm)	Granite	42.941	86.898	3402	1.5	0.9979	32.79 ± 0.41
ARL-10-007	Ala Valley	M5, boulder (125 × 50 × 60 cm)	Granite	42.940	86.898	3398	2.0	0.9980	24.85 ± 0.36
ARL-10-008	Ala Valley	M5, boulder (200 × 140 × 90 cm)	Granite	42.940	86.898	3399	2.0	0.9980	36.24 ± 0.70
DDSL-10-001	Ala Valley	M6, bedrock	Granite (coarse-grain)	42.855	86.898	2933	2.0	0.9962	22.91 ± 0.51
DDSL-10-002	Ala Valley	M6, bedrock	granite (coarse-grain)	42.855	86.898	2926	2.0	0.9962	36.35 ± 0.80
DDSL-10-003	Ala Valley	M6, boulder (200 × 175 × 90 cm)	Granite	42.855	86.898	2922	0.5	0.9979	70.84 ± 1.44
DDSL-10-004	Ala Valley	M6, boulder (100 × 100 × 50 cm)	Granite	42.855	86.898	2927	3.0	0.9979	48.52 ± 0.90
DDSL-10-005	Ala Valley	M6, boulder (105 × 90 × 47 cm)	Granite	42.854	86.898	2921	3.0	0.9972	43.88 ± 0.78
DDSL-10-006	Ala Valley	M6, bedrock		42.855	86.898	2919	3.0	0.9972	21.75 ± 0.83

Table 1 (continued)

Sample ID	Location	Moraine group, type (dimension)	Lithology	Latitude (°N)	Longitude (°E)	Elevation (m a.s.l.)	Thickness (cm)	Topographic shielding factor <sup>a</sup>	<sup>10</sup> Be concentration (10 <sup>5</sup> atoms g <sup>-1</sup> ) <sup>b</sup>
DDSL-10-007	Ala Valley	M6, boulder (240 × 135 × 60 cm)	Granite (coarse-grain)	42.854	86.899	2911	0.5	0.9950	43.96 ± 1.25
DDSL-10-008	Ala Valley	M6, bedrock	Granite (coarse-grain)	42.854	86.899	2911	2.0	0.9960	29.32 ± 1.37
DDSL-10-014	Ala Valley	Ridge, bedrock	Granite (coarse-grain)	42.887	86.849	3385	2.0	0.9987	34.05 ± 1.28
DDSL-10-015	Ala Valley	Ridge, bedrock	Granite (coarse-grain)	42.889	86.849	3396	2.0	0.9986	65.44 ± 0.82
DDSL-10-016	Ala Valley	Ridge, bedrock	Granite (coarse-grain)	42.892	86.847	3450	3.0	0.9991	34.80 ± 0.40
1#-10-18	Daxi Valley	L1A, boulder (230 × 150 × 130 cm)	Granite	43.115	86.825	3686	3.0	0.9718	0.166 ± 0.018
1#-10-19	Daxi Valley	L1A, boulder (70 × 70 × 30 cm)	Granite	43.115	86.825	3691	2.0	0.9718	0.200 ± 0.018
1#-10-20	Daxi Valley	L1A, boulder (360 × 240 × 120 cm)	Gneiss	43.115	86.825	3694	1.0	0.9718	0.193 ± 0.045
1#-10-21	Daxi Valley	L1A, boulder (160 × 140 × 120 cm)	Gneiss	43.115	86.825	3698	3.5	0.9718	0.184 ± 0.022

<sup>a</sup> The topographic shielding was determined from the SRTM DEM using the python tool designed by Li (2013) with 5° intervals in both azimuth and elevation angles.

<sup>b</sup> All samples were measured using the revised ICN standard (07KNSTD, Nishiizumi et al., 2007). Quartz weights, <sup>9</sup>Be carrier masses, and AMS measured <sup>10</sup>Be/<sup>9</sup>Be ratios of these samples are listed in the online appendix.

terminus location for a particular reconstruction (Benn and Lehmkuhl, 2000). Previous studies have demonstrated that TSAM-derived ELAs yield similar results to observed ELAs for small alpine glaciers (e.g. Maisch, 1992). We used the elevations derived from the SRTM DEM to estimate the ELA depression of each glacial event relative to the ELA of modern glaciers in each valley. We also measured the distance from the terminus of modern glaciers to the moraines that have been constrained by <sup>10</sup>Be or OSL dating in Google Earth. This distance provides a first-order estimate for the extent of the glacial event during moraine formation.

#### 4. Results and interpretations

Five samples (AR-10-001 to 005) taken from EC have a wide range of minimum apparent exposure ages from  $4.4 \pm 0.3$  to  $191.8 \pm 10.9$  ka (Table 2). The probability density plot indicates that the oldest and youngest ages are probably outliers (Fig. 4) with the remaining ages spanning from  $17.3 \pm 0.9$  to  $33.6 \pm 1.8$  ka. The extremely young age of  $4.4 \pm 0.3$  ka may be likely due to boulder exhumation, whereas the oldest age of  $191.8 \pm 10.9$  ka may reflect prior exposure. Given the location of these samples (Fig. 2), it is possible that boulders exposed on the ridge and valley sidewall could have been displaced and transported to the sample site. The location of the EC relative to deposits further down the valley also makes it highly unlikely that this cirque was last glaciated at  $191.8 \pm 10.9$  ka because the main valley was glaciated several times since then. The reduced chi-squared statistic is still much higher than 1 after removing these two samples ( $\chi_R^2 = 60.5$ , Fig. 4), so we tentatively assign a range of minimum apparent exposure ages of  $17.3 \pm 0.9$  to  $33.6 \pm 1.8$  ka to this moraine rather than a weighted mean age.

Minimum apparent exposure ages for four samples (AR-10-021 to 024) from M1 range from  $14.2 \pm 0.8$  to  $31.0 \pm 1.7$  ka (Table 2). The age of  $14.2 \pm 0.8$  ka appears to be a young outlier (Fig. 4) that may reflect post-glacial exhumation. The  $\chi_R^2$  value of the remaining three samples is 9.2 (Fig. 4), indicating that the scatter may be caused by post-glacial degradation processes or prior exposure. Therefore, we tentatively assigned a range of minimum apparent exposure ages of  $21.4 \pm 1.5$  to  $31.0 \pm 1.7$  ka for this moraine.

Four samples (AR-10-007, 009, 010, and 011) from M2 produced minimum apparent exposure ages ranging from  $25.0 \pm 1.6$  to  $32.2 \pm 1.8$  ka (Table 2). The probability density plot indicates that the oldest age of  $32.2 \pm 1.8$  ka may not be part of the younger cluster but in light of the fact that there are only four data points it is difficult to rigorously identify this as an outlier. It is possible that a greater number of samples would show a skewed distribution with the oldest age being at the upper end of the distribution. It is interesting that the two pebble samples produced similar ages ( $25.3 \pm 1.3$  and  $26.3 \pm 1.4$  ka), which in turn are similar to one boulder age in this moraine. We do not know the exposure history of these pebbles though. They could have originated from vein quartz within larger boulders, or could have been part of the original moraine.

Minimum apparent exposure ages for seven samples (AR-10-014 to 020) from M3 range from  $22.9 \pm 1.3$  to  $41.4 \pm 2.2$  ka (Table 2). The oldest age ( $41.4 \pm 2.2$  ka) most likely represents a sample with inheritance (Fig. 4). Removing this sample from the dataset results in a  $\chi_R^2$  value of 6.5, indicating some scatter caused by exhumation or prior exposure. We assigned a range of minimum apparent exposure ages of  $22.9 \pm 1.3$  to  $33.1 \pm 2.0$  ka to this moraine. Ignoring the oldest boulder sample, the ages from the other four boulders cluster around 26.6 ka, whereas two pebble samples yielded ages around 32.6 ka ( $32.3 \pm 1.7$  and  $33.1 \pm 2.0$  ka, Fig. 4). Consistently older exposure ages from pebble samples may indicate that boulder samples are more prone to surface erosion on this moraine.

Although the samples from EC and M1-M3 do not consistently produce tight clusters of <sup>10</sup>Be ages, we argue that they can be interpreted as indicating the presence of a glacial event predating 33 to 22 ka. We tentatively assign this glacial event to late MIS 3 to MIS 2. It is noteworthy that <sup>10</sup>Be apparent exposure ages during this period are not significantly affected by our assumption of zero boulder surface erosion. A surface erosion rate of 3 mm/ka, a value previously used in western Tian Shan and Pamir (e.g. Abramowski et al., 2006; Röhringer et al., 2012), will only increase the exposure ages of 30 ka by at most 8%. The reconstructed glacier extended about 10 km from the terminus of the modern glacier to reach 3350 m a.s.l., requiring an ELA depression of ~225 m (the terminus of the modern glacier is at 3800 m a.s.l.).

Seven samples (ARL-10-001 to 005, KXN-10-22, 24) collected from M4 produced minimum apparent surface exposure ages

**Table 2**  
Minimum  $^{10}\text{Be}$  surface exposure ages calculated using different scaling models.

Sample ID	Moraine group, type	Lal (1991)/Stone (2000)	Desilets and Zreda (2003),	Dunai (2001)	Lifton et al. (2005)	Lal (1991)/Stone (2000)
		constant production rate	Desilets et al. (2006)			Time-dependent production rate
		Exposure age (ka)	Exposure age (ka)	Exposure age (ka)	Exposure age (ka)	Exposure age (ka)
AR-10-001	Cirque, boulder	209.4 ± 11.9	162.2 ± 9.2	159.8 ± 9.1	156.2 ± 8.8	191.8 ± 10.9
AR-10-002	Cirque, boulder	29.8 ± 2.1	24.9 ± 1.8	24.8 ± 1.8	24.5 ± 1.8	28.6 ± 2.1
AR-10-003	Cirque, boulder	4.3 ± 0.3	4.0 ± 0.3	4.2 ± 0.3	3.9 ± 0.3	4.4 ± 0.3
AR-10-004	Cirque, boulder	17.6 ± 0.9	15.3 ± 0.8	15.4 ± 0.8	15.1 ± 0.8	17.3 ± 0.9
AR-10-005	Cirque, boulder	35.5 ± 1.9	29.2 ± 1.6	29.1 ± 1.6	28.7 ± 1.5	33.6 ± 1.8
AR-10-021	M1, pebbles	27.7 ± 1.6	23.3 ± 1.3	23.3 ± 1.3	22.9 ± 1.3	26.7 ± 1.5
AR-10-022	M1, boulder	32.5 ± 1.8	27.1 ± 1.5	27.0 ± 1.5	26.6 ± 1.5	31.0 ± 1.7
AR-10-023	M1, boulder	22.0 ± 1.5	18.8 ± 1.3	18.9 ± 1.3	18.6 ± 1.3	21.4 ± 1.5
AR-10-024	M1, boulder	14.3 ± 0.8	12.6 ± 0.7	12.8 ± 0.7	12.5 ± 0.7	14.2 ± 0.8
AR-10-007	M2, boulder	25.8 ± 1.7	22.1 ± 1.4	22.1 ± 1.5	21.7 ± 1.4	25.0 ± 1.6
AR-10-009	M2, pebbles	26.2 ± 1.3	22.4 ± 1.1	22.4 ± 1.1	22.0 ± 1.1	25.3 ± 1.3
AR-10-010	M2, pebbles	27.3 ± 1.5	23.2 ± 1.3	23.2 ± 1.3	22.9 ± 1.3	26.3 ± 1.4
AR-10-011	M2, boulder	33.8 ± 1.8	28.3 ± 1.6	28.2 ± 1.6	27.8 ± 1.5	32.2 ± 1.8
AR-10-014	M3, boulder	23.6 ± 1.3	20.3 ± 1.2	20.3 ± 1.2	20.0 ± 1.1	22.9 ± 1.3
AR-10-015	M3, boulder	26.5 ± 1.4	22.7 ± 1.3	22.7 ± 1.3	22.3 ± 1.2	25.6 ± 1.4
AR-10-016	M3, boulder	29.1 ± 1.6	24.6 ± 1.4	24.6 ± 1.4	24.2 ± 1.3	27.9 ± 1.5
AR-10-017	M3, boulder	27.7 ± 1.5	23.5 ± 1.3	23.5 ± 1.3	23.2 ± 1.3	26.7 ± 1.4
AR-10-018	M3, boulder	44.3 ± 2.3	36.4 ± 1.9	36.3 ± 1.9	35.6 ± 1.9	41.4 ± 2.2
AR-10-019	M3, pebbles	33.9 ± 1.8	28.5 ± 1.5	28.4 ± 1.5	28.0 ± 1.5	32.3 ± 1.7
AR-10-020	M3, pebbles	34.8 ± 2.0	29.1 ± 1.7	29.0 ± 1.7	28.6 ± 1.7	33.1 ± 2.0
ARL-10-001	M4, boulder	56.7 ± 3.0	46.5 ± 2.5	46.2 ± 2.5	45.0 ± 2.4	52.9 ± 2.8
ARL-10-002	M4, boulder	48.7 ± 2.7	40.3 ± 2.2	40.2 ± 2.2	39.3 ± 2.2	45.3 ± 2.5
ARL-10-003	M4, boulder	51.5 ± 2.8	42.5 ± 2.3	42.3 ± 2.3	41.3 ± 2.2	47.9 ± 2.6
ARL-10-004	M4, boulder	42.3 ± 2.3	35.5 ± 1.9	35.3 ± 1.9	34.7 ± 1.9	39.7 ± 2.1
ARL-10-005	M4, boulder	52.6 ± 2.9	43.3 ± 2.4	43.2 ± 2.4	42.1 ± 2.3	49.0 ± 2.7
KXN-10-022	M4, boulder	90.3 ± 4.7	74.1 ± 3.9	73.5 ± 3.8	72.0 ± 3.8	84.4 ± 4.4
KXN-10-024	M4, boulder	39.3 ± 3.0	33.1 ± 2.5	33.0 ± 2.5	32.4 ± 2.5	37.0 ± 2.8
ARL-10-006	M5, boulder	74.6 ± 3.8	60.9 ± 3.1	60.4 ± 3.1	59.2 ± 3.0	69.7 ± 3.5
ARL-10-007	M5, boulder	56.7 ± 2.9	46.0 ± 2.4	45.8 ± 2.4	44.6 ± 2.3	52.9 ± 2.7
ARL-10-008	M5, boulder	83.2 ± 4.4	67.6 ± 3.6	67.0 ± 3.6	65.7 ± 3.5	77.6 ± 4.1
DDSL-10-001	M6, bedrock	69.4 ± 3.7	58.9 ± 3.2	58.5 ± 3.2	57.3 ± 3.1	65.2 ± 3.5
DDSL-10-002	M6, bedrock	111.7 ± 6.1	93.8 ± 5.1	93.0 ± 5.1	91.4 ± 5.0	103.8 ± 5.7
DDSL-10-003	M6, boulder	221.0 ± 12.2	182.3 ± 10.1	180.6 ± 10.0	176.8 ± 9.8	203.1 ± 11.2
DDSL-10-004	M6, boulder	151.5 ± 8.1	125.0 ± 6.7	124.1 ± 6.7	121.1 ± 6.5	139.4 ± 7.5
DDSL-10-005	M6, boulder	137.1 ± 7.3	113.8 ± 6.1	112.9 ± 6.0	110.4 ± 5.9	126.3 ± 6.7
DDSL-10-006	M6, bedrock	66.9 ± 4.2	56.8 ± 3.6	56.5 ± 3.6	55.1 ± 3.5	62.9 ± 3.9
DDSL-10-007	M6, boulder	135.6 ± 7.8	112.7 ± 6.5	111.8 ± 6.5	109.4 ± 6.3	124.9 ± 7.2
DDSL-10-008	M6, bedrock	90.5 ± 6.2	76.3 ± 5.2	75.8 ± 5.2	74.3 ± 5.1	84.7 ± 5.8
DDSL-10-014	Ridge, bedrock	78.7 ± 4.9	64.2 ± 4.0	63.7 ± 4.0	62.4 ± 3.9	73.5 ± 4.6
DDSL-10-015	Ridge, bedrock	153.2 ± 7.9	121.6 ± 6.3	120.4 ± 6.3	117.6 ± 6.1	140.4 ± 7.3
DDSL-10-016	Ridge, bedrock	78.1 ± 3.9	63.4 ± 3.2	62.8 ± 3.2	61.7 ± 3.1	72.9 ± 3.7
1#-10-18	LIA, boulder	0.33 ± 0.04	0.33 ± 0.04	0.32 ± 0.04	0.33 ± 0.04	0.36 ± 0.04
1#-10-19	LIA, boulder	0.39 ± 0.04	0.40 ± 0.04	0.38 ± 0.04	0.40 ± 0.04	0.43 ± 0.05
1#-10-20	LIA, boulder	0.37 ± 0.09	0.38 ± 0.09	0.36 ± 0.09	0.38 ± 0.09	0.41 ± 0.10
1#-10-21	LIA, boulder	0.36 ± 0.05	0.37 ± 0.05	0.35 ± 0.05	0.37 ± 0.05	0.40 ± 0.05

**Note:** All ages were calculated using the CRONUS-Earth 2.2 online calculator (Balco et al., 2008) assuming zero boulder surface erosion, implying a minimum surface exposure age. The calculation was based on the reference  $^{10}\text{Be}$  production rate of the calibration dataset from Balco et al. (2009; NENA). The rock density was assumed as 2.7 g/cm<sup>3</sup>. External uncertainty was reported at the 1 $\sigma$  level.

ranging from 37.0 ± 2.8 to 84.4 ± 4.4 ka (Table 2, Fig. 4). The oldest age of 84.4 ± 4.4 ka likely represents an outlier with inheritance from prior exposure. Removing this age from the dataset results in a  $\chi^2_R$  value of 5.2, indicating that the remaining ages may be affected by post-glacial processes or prior exposure, and so we assign a range of minimum apparent exposure ages of 37.0 ± 2.8 to 52.9 ± 2.8 ka to this moraine. The impact of a boulder surface erosion rate of 3 mm/ka on derived exposure ages is most likely <15%. Hence, the minimum age estimates are consistent with a MIS 3 stage for the glacial expansion. Because the glacier extended >20 km beyond its current extent and the lowest elevation reached was about 2950 m a.s.l., representing an ELA depression of ~425 m, this event was much more extensive than the glacial event during late MIS 3 to MIS 2.

Minimum apparent exposure ages for three samples taken from erratic boulders on M5 (ARL-10-006 to 008) range from 52.9 ± 2.7 to 77.6 ± 4.1 ka with a  $\chi^2_R$  value of 6.2 (Table 2, Fig. 4). Because this location is characterized by the presence of till remnants and

associated erratics, and an absence of landforms, we infer that these sites are highly degraded. Hence, the oldest age of 77.6 ± 4.1 ka is most likely the best representation of the formation age of this till (Heyman et al., 2011b), indicating a glacial event during MIS 4. During this glacial event, we infer that at least the lower parts of the interfluvies were covered by ice because the samples were taken from such a location. The glacier was more extensive during this event than during the M4 glacial event; however, because a M5 terminal moraine is absent, we can only infer that the ELA depression for the M5 glacier was probably larger than for the M4 glacier, and therefore exceeded 425 m.

Four boulder samples collected from M6 (DDSL-10-003 to 005 and 007) yielded minimum apparent exposure ages ranging from 124.9 ± 7.2 to 203.1 ± 11.2 ka (Table 2). The probability density plot of these ages (Fig. 4) indicates a tight cluster ( $\chi^2_R = 1.2$ ) around a weighted mean of 130.2 ± 9.7 ka if the oldest age of 203.1 ± 11.2 ka is removed as an outlier. These ages represent the largest and oldest glacial event in the Ala Valley and are therefore strongly affected by

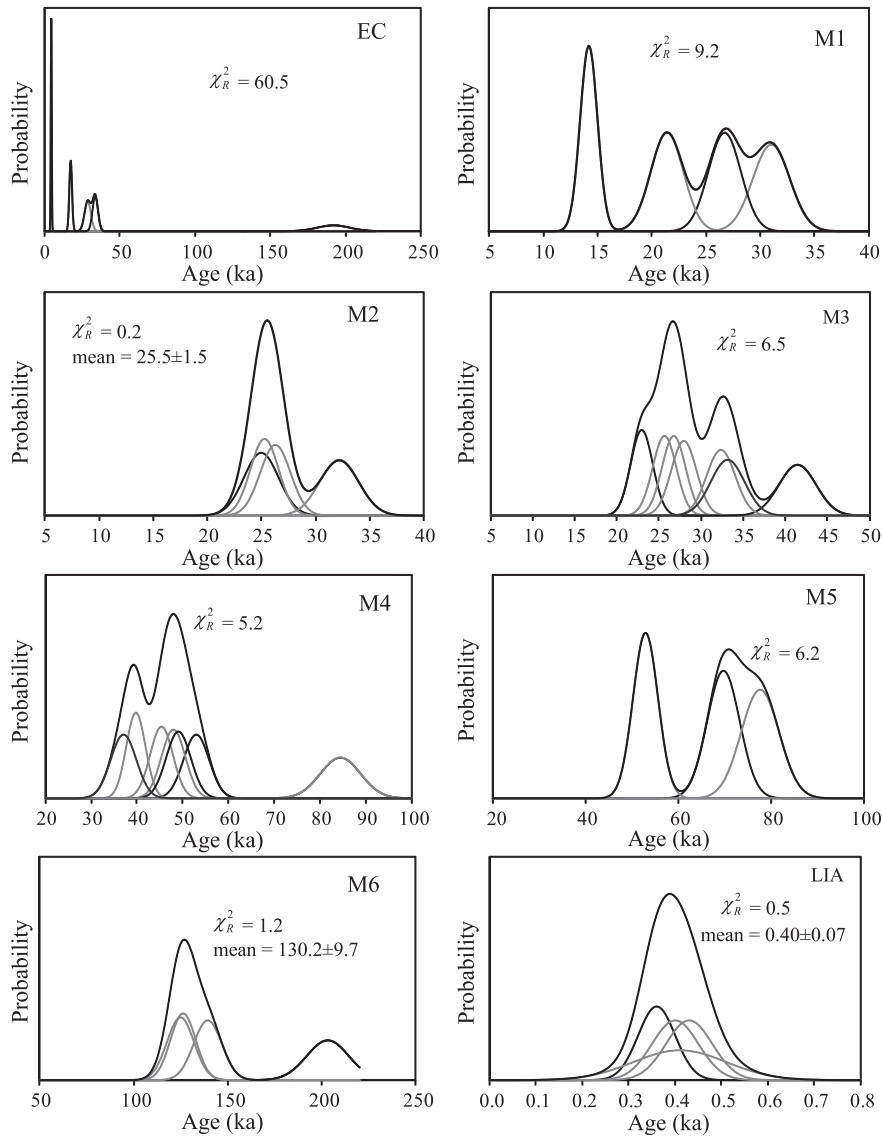


**Fig. 4.** Probability density plot of <sup>10</sup>Be surface exposure ages for each moraine/setting and the value of the reduced chi-squared statistic ( $\chi^2_R$ ) after removing outliers. The weighted mean age for M2, M6 and LIA are listed because  $\chi^2_R$  is less than or close to 1.

surface erosion. For example, a surface erosion rate of 3 mm/ka will shift the youngest apparent exposure age of  $124.9 \pm 7.2$  ka to  $>180$  ka and the oldest apparent exposure age of  $203.1 \pm 11.2$  ka to  $>580$  ka. These ages most likely represent a glacial event during MIS 6 or older. As with M5, we can only infer that the minimum ELA

depression for the glacier that deposited the M6 boulders exceeded 425 m.

Comparison of bedrock and erratic apparent exposure ages has been used to quantify the pattern of glacial erosion. In particular, if bedrock ages are older than the ages of adjacent erratics, the

**Table 3**  
Maximum surface erosion rates (cm/ka) derived from bedrock samples in the Tianger Range, eastern Tian Shan, China.

Sample ID	Lal (1991)/Stone (2000)	Desilets and Zreda (2003),	Dunai (2001)	Lifton et al. (2005)	Lal (1991)/Stone (2000)
	constant production rate	Desilets et al. (2006)			Time-dependent production rate
	Erosion rate (cm/ka)	Erosion rate (cm/ka)	Erosion rate (cm/ka)	Erosion rate (cm/ka)	Erosion rate (cm/ka)
DDSL-10-001	$10.2 \pm 0.9$	$11.3 \pm 1.3$	$11.3 \pm 1.3$	$11.7 \pm 1.2$	$10.8 \pm 0.9$
DDSL-10-002	$6.3 \pm 0.6$	$7.0 \pm 0.8$	$7.0 \pm 0.8$	$7.3 \pm 0.7$	$6.7 \pm 0.6$
DDSL-10-006	$10.6 \pm 1.0$	$11.7 \pm 1.4$	$11.7 \pm 1.4$	$12.2 \pm 1.3$	$11.2 \pm 1.0$
DDSL-10-008	$7.8 \pm 0.8$	$8.6 \pm 1.1$	$8.7 \pm 1.1$	$9.0 \pm 1.0$	$8.3 \pm 0.8$
DDSL-10-014	$8.9 \pm 0.8$	$10.2 \pm 1.3$	$10.3 \pm 1.3$	$10.6 \pm 1.1$	$9.4 \pm 0.9$
DDSL-10-015	$4.5 \pm 0.4$	$5.2 \pm 0.6$	$5.3 \pm 0.6$	$5.5 \pm 0.6$	$4.8 \pm 0.4$
DDSL-10-016	$8.9 \pm 0.8$	$10.3 \pm 1.2$	$10.4 \pm 1.2$	$10.8 \pm 1.1$	$9.5 \pm 0.8$

**Note:** All erosion rates were calculated using the CRONUS-Earth 2.2 online calculator (Balco et al., 2008) assuming a long-term continuous exposure of the bedrock surface, representing the maximum erosion rate of the bedrock surface (Lal, 1991).

**Table 4**  
Recalculated previously published minimum  $^{10}\text{Be}$  surface exposure ages across the Tian Shan.

Sample ID	Location	Latitude (°N)	Longitude (°E)	Elevation (m a.s.l.)	Thickness (cm)	Topographic shielding factor	$^{10}\text{Be}$ concentration ( $10^5$ atoms $\text{g}^{-1}$ )	Published $^{10}\text{Be}$ age (ka)	Recalculated $^{10}\text{Be}$ age (ka)	Publication
TB1	Daxi Valley	43.114	86.843	3558	3.0	0.990	$5.98 \pm 0.38$	$9.6 \pm 0.9$	$11.5 \pm 0.9$	Kong et al. (2009)
TB2		43.114	86.843	3567	3.0	0.990	$9.09 \pm 0.42$	$14.6 \pm 1.2$	$17.2 \pm 1.2$	
TB3		43.114	86.843	3562	3.0	0.990	$11.17 \pm 0.72$	$17.9 \pm 1.7$	$21.0 \pm 1.7$	
TB4		43.114	86.843	3561	3.0	0.990	$12.97 \pm 0.71$	$20.9 \pm 1.9$	$24.3 \pm 1.8$	
TB5		43.113	86.845	3530	3.0	0.990	$9.34 \pm 0.23$	$15.3 \pm 1.1$	$18.0 \pm 1.0$	
TB7		43.114	86.847	3511	3.0	0.990	$8.88 \pm 0.42$	$14.7 \pm 1.2$	$17.3 \pm 1.2$	
TB8		43.114	86.847	3511	3.0	0.990	$8.39 \pm 0.49$	$13.9 \pm 1.3$	$16.4 \pm 1.3$	
TD2		43.116	86.929	3164	3.0	0.980	$9.87 \pm 0.43$	$20.1 \pm 1.7$	$23.5 \pm 1.5$	
TD5		43.100	86.928	3170	3.0	0.980	$7.57 \pm 0.45$	$15.4 \pm 1.4$	$18.2 \pm 1.4$	
TD6		43.121	86.856	3449	3.0	0.990	$8.87 \pm 0.25$	$15.2 \pm 1.2$	$17.9 \pm 1.0$	
TA1		43.114	86.921	3389	3.0	1.000	$5.73 \pm 0.42$	$10.1 \pm 1.0$	$12.0 \pm 1.1$	
TA2		43.113	86.920	3405	3.0	1.000	$2.97 \pm 0.30$	$5.2 \pm 0.6$	$6.2 \pm 0.7$	
TA4		43.113	86.920	3408	3.0	1.000	$9.54 \pm 0.88$	$16.6 \pm 1.9$	$19.5 \pm 2.0$	
TA6		43.113	86.920	3423	3.0	1.000	$5.27 \pm 0.54$	$9.1 \pm 1.1$	$10.8 \pm 1.2$	
TA10		43.113	86.924	3324	3.0	1.000	$5.39 \pm 0.40$	$9.8 \pm 1.0$	$11.7 \pm 1.0$	
TS-07-13	Daxi Valley	43.114	86.847	3520	2.0	0.982	$8.51 \pm 0.40$	$15.9 \pm 1.5$	$17.9 \pm 1.2$	Li et al. (2011)
TS-07-15		43.114	86.847	3520	2.0	0.982	$8.35 \pm 0.19$	$15.6 \pm 1.4$	$17.5 \pm 0.9$	
TS-07-21		43.119	86.867	3429	3.0	0.975	$8.26 \pm 0.31$	$16.4 \pm 1.5$	$18.5 \pm 1.1$	
TS-07-23		43.119	86.825	3831	2.0	0.978	$9.97 \pm 0.21$	$15.7 \pm 1.4$	$17.7 \pm 0.9$	
TS-07-25		43.119	86.824	3832	3.0	0.978	$9.00 \pm 0.42$	$14.3 \pm 1.4$	$16.2 \pm 1.1$	
TS-07-28		43.110	86.945	3005	2.5	0.944	$7.13 \pm 0.30$	$18.7 \pm 1.8$	$21.0 \pm 1.4$	
TS-07-29		43.110	86.945	3006	2.5	0.944	$6.15 \pm 0.25$	$16.2 \pm 1.5$	$18.2 \pm 1.2$	
TS-07-35		43.119	86.920	3192	2.0	0.955	$6.60 \pm 0.11$	$15.3 \pm 1.3$	$17.2 \pm 0.9$	
TS-07-36		43.119	86.920	3186	2.0	0.955	$7.39 \pm 0.13$	$17.1 \pm 1.5$	$19.3 \pm 1.0$	
TS-07-37		43.119	86.920	3183	3.5	0.955	$7.01 \pm 0.18$	$16.5 \pm 1.5$	$18.6 \pm 1.0$	
TS-07-38		43.119	86.920	3179	3.0	0.955	$6.37 \pm 0.14$	$15.0 \pm 1.3$	$16.9 \pm 0.9$	
AK11	Aksu Valley	39.680	70.050	2240	4.0	0.974	$4.62 \pm 0.36$	$16.3 \pm 2.1$	$21.2 \pm 2.0$	Abramowski et al. (2006)
AK12		39.680	70.050	2240	4.0	0.974	$6.38 \pm 0.35$	$22.1 \pm 2.6$	$28.8 \pm 2.1$	
AK13		39.680	70.050	2240	4.0	0.974	$4.87 \pm 0.42$	$17.1 \pm 2.3$	$22.3 \pm 2.2$	
AK21		39.640	70.060	2900	4.0	0.977	$8.21 \pm 0.56$	$18.8 \pm 2.4$	$24.5 \pm 2.1$	
AK22		39.640	70.060	2900	4.0	0.977	$4.47 \pm 0.33$	$10.3 \pm 1.3$	$13.7 \pm 1.2$	
AK23		39.640	70.060	2900	4.0	0.977	$5.51 \pm 0.47$	$12.8 \pm 1.7$	$16.8 \pm 1.7$	
AK24		39.640	70.060	2900	4.0	0.977	$6.86 \pm 0.45$	$15.8 \pm 2.0$	$20.7 \pm 1.7$	
AK25		39.640	70.060	2900	4.0	0.977	$6.90 \pm 0.42$	$15.9 \pm 1.9$	$20.8 \pm 1.6$	
AK31		39.650	70.060	2860	4.0	0.981	$3.91 \pm 0.24$	$9.2 \pm 1.1$	$12.3 \pm 1.0$	
AK32		39.650	70.060	2860	4.0	0.981	$10.32 \pm 0.55$	$23.8 \pm 2.8$	$31.0 \pm 2.2$	
AK33		39.650	70.060	2860	4.0	0.981	$8.45 \pm 0.45$	$19.7 \pm 2.3$	$25.7 \pm 1.9$	
AK34		39.650	70.060	2860	4.0	0.981	$6.91 \pm 0.52$	$16.3 \pm 2.1$	$21.2 \pm 1.9$	
AK35		39.650	70.060	2860	4.0	0.981	$5.22 \pm 0.36$	$12.4 \pm 1.6$	$16.2 \pm 1.4$	
AK41		39.640	70.050	2930	4.0	0.989	$9.95 \pm 0.51$	$22 \pm 2.6$	$28.5 \pm 2.0$	
AK42		39.640	70.050	2930	6.0	0.989	$8.15 \pm 0.38$	$18.4 \pm 2.1$	$24.0 \pm 1.6$	
AK43		39.640	70.050	2930	8.0	0.989	$7.74 \pm 0.47$	$17.7 \pm 2.1$	$23.2 \pm 1.8$	
AK44		39.640	70.050	2930	5.0	0.989	$8.37 \pm 0.47$	$18.8 \pm 2.2$	$24.4 \pm 1.8$	
AK45		39.640	70.050	2930	4.0	0.989	$6.31 \pm 0.31$	$14.3 \pm 1.7$	$18.5 \pm 1.3$	
AV1	Koksu Valley	39.680	71.620	3440	4.0	1.000	$6.23 \pm 0.41$	$10.3 \pm 1.3$	$13.8 \pm 1.1$	Abramowski et al. (2006)
AV2		39.680	71.620	3440	4.0	1.000	$6.27 \pm 0.39$	$10.3 \pm 1.3$	$13.9 \pm 1.1$	
AV3		39.680	71.620	3440	4.0	1.000	$6.37 \pm 0.40$	$10.5 \pm 1.3$	$14.1 \pm 1.1$	
KK1		39.550	72.080	2500	4.0	1.000	$18.50 \pm 0.87$	$50.1 \pm 5.8$	$68.4 \pm 4.7$	
KK2		39.550	72.080	2500	4.0	1.000	$20.19 \pm 0.94$	$55.1 \pm 6.4$	$74.8 \pm 5.1$	
KK3		39.550	72.080	2500	4.0	1.000	$17.27 \pm 0.76$	$46.6 \pm 5.3$	$64.0 \pm 4.3$	
SCT-020901-2	Gulbel Pass	42.030	77.190	3283	1.0	0.992	$20.11 \pm 0.49$	$40.5 \pm 3.1$	$42.3 \pm 2.3$	Koppes et al. (2008)
SCT-020901-3		42.030	77.190	3283	1.0	0.992	$16.23 \pm 0.41$	$32.4 \pm 2.4$	$34.7 \pm 1.9$	
SCT-020901-4		42.040	77.210	3140	1.0	0.992	$13.88 \pm 0.35$	$30.0 \pm 2.3$	$32.4 \pm 1.8$	
SCT-020901-5		42.040	77.210	3140	1.0	0.992	$19.10 \pm 0.57$	$41.9 \pm 3.3$	$43.7 \pm 2.5$	
SCT-030901-6		42.040	77.120	2759	1.0	0.992	$33.48 \pm 0.80$	$98.1 \pm 7.9$	$98.2 \pm 5.4$	
KTS98-CS-61b	Djo Bog Gulsh Valley	41.000	76.050	3804	3.0	0.990	$5.07 \pm 0.15$	$7.6 \pm 0.6$	$8.9 \pm 0.5$	Koppes et al. (2008)
KTS98-CS-62a		41.000	76.050	3879	3.0	0.990	$3.20 \pm 0.10$	$4.6 \pm 0.3$	$5.4 \pm 0.3$	
KTS98-CS-62b		41.000	76.050	3879	3.0	0.989	$3.05 \pm 0.09$	$4.4 \pm 0.3$	$5.2 \pm 0.3$	
KTS98-CS-66		40.980	76.150	3576	4.0	0.996	$20.58 \pm 0.35$	$36.5 \pm 2.7$	$38.4 \pm 2.0$	
KTS98-CS-81	Terekçu Valley	41.050	75.730	2598	1.0	0.998	$10.32 \pm 0.25$	$31.6 \pm 2.4$	$34.1 \pm 1.9$	Koppes et al. (2008)
KTS98-CS-83		41.050	75.730	2598	1.0	0.998	$16.77 \pm 0.42$	$52.5 \pm 4.0$	$54.8 \pm 3.0$	
KTS98-CS-87	Ala Bash Basin	42.080	76.460	2496	0.5	0.997	$19.35 \pm 0.23$	$64.0 \pm 4.8$	$66.4 \pm 3.4$	Koppes et al. (2008)
KTS98-CS-88		42.080	76.460	2496	4.0	0.997	$20.40 \pm 0.34$	$69.9 \pm 5.3$	$72.0 \pm 3.8$	
KTS98-CS-90		42.080	76.460	2403	7.0	0.998	$33.77 \pm 1.49$	$134.6 \pm 12.7$	$129.6 \pm 8.8$	
KTS98-CS-91		42.080	76.460	2403	2.0	1.000	$41.60 \pm 0.97$	$163.5 \pm 14.1$	$154.3 \pm 8.6$	

Table 4 (continued)

Sample ID	Location	Latitude (°N)	Longitude (°E)	Elevation (m a.s.l.)	Thickness (cm)	Topographic shielding factor	$^{10}\text{Be}$ concentration ( $10^5$ atoms $\text{g}^{-1}$ )	Published $^{10}\text{Be}$ age (ka)	Recalculated $^{10}\text{Be}$ age (ka)	Publication
KTS98-CS-92		42.080	76.460	2403	5.0	0.994	$19.05 \pm 0.46$	$70.2 \pm 5.5$	$72.4 \pm 4.0$	
KTS98-CS-93		42.080	76.450	2229	5.0	0.994	$22.95 \pm 0.62$	$97.7 \pm 8.0$	$98.4 \pm 5.6$	
KTS98-CS-94		42.080	76.450	2229	2.5	1.000	$25.88 \pm 0.73$	$108.4 \pm 9.0$	$107.7 \pm 6.2$	
KTS98-CS-95		42.080	76.450	2229	3.5	1.000	$31.90 \pm 0.62$	$139.0 \pm 11.5$	$133.7 \pm 7.2$	
KTS98-CS-96		42.080	76.450	2229	10.0	1.000	$16.81 \pm 0.40$	$72.2 \pm 5.7$	$74.5 \pm 4.1$	
KTS98-CS-97		42.050	76.430	2850	1.0	0.998	$34.00 \pm 0.79$	$93.0 \pm 7.4$	$93.6 \pm 5.1$	
KTS98-CS-98		42.050	76.430	2850	2.0	0.998	$18.99 \pm 0.45$	$50.1 \pm 3.8$	$52.1 \pm 2.8$	
KTS98-CS-99		42.050	76.430	3750	2.0	0.996	$2.26 \pm 0.07$	$3.4 \pm 0.3$	$4.0 \pm 0.2$	
KTS98-CS-100		42.050	76.430	3750	6.0	0.996	$11.32 \pm 0.27$	$17.8 \pm 1.3$	$19.9 \pm 1.1$	
KTS98-CS-101	Ala Archa Valley	42.520	74.510	3246	2.0	0.929	$0.12 \pm 0.03$	$0.25 \pm 0.1$	$0.32 \pm 0.08$	Koppes et al. (2008)
KTS98-CS-102		42.520	74.510	3180	1.5	0.913	$0.25 \pm 0.04$	$0.54 \pm 0.1$	$0.69 \pm 0.12$	
KTS98-CS-104	Chor Kyrchak Valley	42.63	74.61	2040	3.0	0.997	$10.90 \pm 0.39$	$48.7 \pm 4.0$	$48.6 \pm 3.0$	Koppes et al. (2008)
KI11	Kitschi-Kurumdu Valley	40.783	75.488	3870	3.0	1.000	$6.19 \pm 0.25$	$9.3 \pm 0.9$	$10.5 \pm 0.7$	Zech (2012)
KI12		40.783	75.488	3870	3.0	1.000	$9.87 \pm 0.35$	$14.7 \pm 1.4$	$16.6 \pm 1.0$	
KI13		40.783	75.487	3870	3.0	1.000	$10.54 \pm 0.32$	$15.7 \pm 1.4$	$17.7 \pm 1.0$	
KI14		40.783	75.487	3870	3.0	1.000	$9.34 \pm 0.45$	$14.0 \pm 1.4$	$15.7 \pm 1.1$	
KI21		40.787	75.473	3990	3.0	1.000	$13.58 \pm 0.47$	$18.8 \pm 1.7$	$21.2 \pm 1.3$	
KI22		40.787	75.473	3995	3.0	1.000	$15.60 \pm 0.53$	$21.4 \pm 2.0$	$24.1 \pm 1.4$	
KI23		40.787	75.473	3980	3.0	1.000	$11.39 \pm 0.36$	$16.0 \pm 1.4$	$18.0 \pm 1.0$	
KI24		40.784	75.476	3940	3.0	1.000	$11.02 \pm 0.36$	$15.8 \pm 1.4$	$17.8 \pm 1.0$	
KI25		40.784	75.476	3940	3.0	1.000	$12.55 \pm 0.42$	$17.9 \pm 1.6$	$20.1 \pm 1.2$	
KI31		40.765	75.503	3725	3.0	1.000	$34.87 \pm 1.05$	$52.8 \pm 4.8$	$60.3 \pm 3.5$	
KI32		40.765	75.503	3725	3.0	1.000	$36.88 \pm 1.44$	$56.1 \pm 5.3$	$63.7 \pm 4.0$	
KI33		40.764	75.502	3720	3.0	1.000	$10.28 \pm 0.41$	$16.6 \pm 1.5$	$18.6 \pm 1.2$	
KI34		40.767	75.508	3708	3.0	1.000	$17.51 \pm 0.53$	$27.6 \pm 2.5$	$31.0 \pm 1.8$	

**Note:** Ages were recalculated using the CRONUS-Earth 2.2 online calculator (Balco et al., 2008) assuming zero boulder surface erosion and using the time-dependent production rate scaling model of Lal (1991)/Stone (2000). The calculation was based on the reference  $^{10}\text{Be}$  production rate of the calibration dataset from Balco et al. (2009; NENA). The rock density was assumed as  $2.7 \text{ g/cm}^3$ . External uncertainties were reported at the  $1\sigma$  level.

inheritance signal can be used to back calculate an erosion depth (Stroeven et al., 2002; Fabel et al., 2004; Li et al., 2005). However, at M6, minimum apparent exposure ages from four coarse-grained granite bedrock samples (DDSL-10-001, 002, 006 and 008) are consistently younger than the minimum apparent exposure ages from the nearby four fine-grained granite erratic boulders (DDSL-10-003 to 005 and 007, Table 2). Shielding by sediment cover in the past could cause an underestimation in exposure age but we believe geomorphic conditions argue against it. These bedrock ages are consistent with ages from three coarse-grained granite bedrock samples taken from interfluvial ridges (DDSL-10-014 to 016,  $72.9 \pm 3.7$  to  $140.4 \pm 7.3$ , Table 2), which are unlikely to have been covered by sediment. The apparently younger exposure ages from bedrock samples are most likely due to the difference in granite composition (Fig. 3F, G): the coarse-grained bedrock samples simply weathered faster than the fine-grained boulder samples. Assuming continuous exposure and ignoring ice cover effects, the range of maximum erosion rates derived from these bedrock surfaces is  $6.7 \pm 0.6$  to  $11.2 \pm 1.0 \text{ cm/ka}$ , similar to the range of maximum erosion rates derived from the three interfluvial bedrock samples (DDSL-10-014 to 016,  $4.8 \pm 0.4$  to  $9.5 \pm 0.8 \text{ cm/ka}$ ; Table 3). These values are an indicator of bedrock erosion rates (or landscape lowering rates) for the mountain range in this region.

In the Daxi Valley, four boulder samples from the outermost fresh moraine in front of Glacier No. 1 (1#-10-18 to 21) yielded tightly clustered minimum apparent exposure ages ranging from  $0.36 \pm 0.04$  to  $0.43 \pm 0.05 \text{ ka}$  (Table 2) with a weighted mean of  $0.40 \pm 0.07 \text{ ka}$  ( $\chi^2_R = 0.5$ ; Fig. 4). This age is consistent with ages determined by lichenometry (Chen, 1989) and AMS  $^{14}\text{C}$  (Yi et al., 2004) and indicates that Glacier No. 1 advanced during the LIA in response to an ELA depression of about 50–80 m (calculated based on the terminal elevations of the two branches of Glacier No. 1). These ages also shed some light on processes that affect the distribution of ages we observed on other moraines. At least for this

moraine four samples yielded a tight cluster, with no evidence of prior exposure.

## 5. Discussion

### 5.1. Chronology of Quaternary glaciations in the Tian Shan

Our results indicate five major glacial events on the northern and southern slopes of the Tianger Range during MIS 6 or older, 4, 3, 2, and 1 (LIA) (Fig. 5). This glacial chronology is consistent with glacial chronologies derived from the western Tian Shan (Abramowski et al., 2006; Koppes et al., 2008; Zech, 2012). For the maximum glaciation, Koppes et al. (2008) obtained three  $^{10}\text{Be}$  minimum apparent exposure ages from the Ala Bash Basin in the Terskey Ala Tau Range of the western Tian Shan (Fig. 1) which they interpreted as MIS 5 but which, when recalculated, fall between  $72.4 \pm 4.0$  and  $154.3 \pm 8.6 \text{ ka}$  (Table 4). These ages are consistent with our M6 ages in the eastern Tian Shan, suggesting the existence of a penultimate glaciation (MIS 6 or older) in different parts of the Tian Shan. The local LGM in the eastern Tian Shan has been dated to at least  $77.6 \pm 4.1 \text{ ka}$ , which is consistent with the three recalculated  $^{10}\text{Be}$  minimum apparent exposure ages from the Koku Valley in the Alay Range of the Kyrgyz Tian Shan ranging from  $64.0 \pm 4.3$  to  $74.8 \pm 5.1 \text{ ka}$  (Abramowski et al., 2006) and two  $^{10}\text{Be}$  minimum apparent exposure ages from the Ala Bash Basin of  $66.4 \pm 3.4$  and  $72.0 \pm 3.8 \text{ ka}$  (Koppes et al., 2008, Table 4). Zech (2012) obtained four  $^{10}\text{Be}$  minimum apparent exposure ages from moraines in the Kitschi-Kurumdu Valley, Kyrgyzstan (Fig. 1), ranging from  $18.6 \pm 1.2$  to  $63.7 \pm 4.0 \text{ ka}$  (recalculated ages, Table 4), and he concluded that these moraines were formed before  $63.7 \text{ ka}$  (recalculated age). Narama et al. (2009) defined a Terskey Stage I in the Kyrgyz Tian Shan as being from 56 to 76 ka based on three OSL ages. Taken together, these results indicate that the local LGM across the Tian Shan occurred during MIS 4.

Our  $^{10}\text{Be}$  ages indicate a significant glacial event during MIS 3 (37–53 ka) in the eastern Tian Shan. A similar glacial event has also been found in the western Tian Shan, for example, [Koppes et al. \(2008\)](#) reported a single minimum apparent exposure age of  $54.8 \pm 3.0$  ka for a moraine in the Terekçu Valley in the At Bashi Range ([Fig. 1](#)), a  $^{10}\text{Be}$  minimum apparent exposure age of  $48.6 \pm 3.0$  ka on a moraine in the Chor Kyrchak Valley in the Kyrgyz Front Range (adjacent to the Ala Archa Valley; [Fig. 1](#)), and four minimum apparent exposure ages from moraines near Gulbel Pass in the Terskey Ala Tau Range ([Fig. 1](#)) that range from  $32.4 \pm 1.8$  to  $43.7 \pm 2.5$  ka (all recalculated ages; [Table 4](#)). All these locations support the existence of a MIS 3 glacial event across the Tian Shan.

The late MIS 3 to MIS 2 glacial event in the eastern Tian Shan was dated from 22 to 33 ka ([Fig. 5](#)). The latter part of this glacial event corresponds to gLGM (26.5–19 ka) ([Clark et al., 2009](#)). The early part of this glacial event apparently predated the gLGM by a few thousand years, but is consistent with the more extensive duration of a cold period recorded in the Guliya ice core record on the northern Tibetan Plateau ( $35^{\circ}17' \text{ N}$ ,  $81^{\circ}29' \text{ E}$ ) to have occurred between 18 and 32 ka ([Thompson et al., 1997](#)). MIS 2 glacial events have also been identified in the western Tian Shan. For example, [Abramowski et al. \(2006\)](#) obtained ten  $^{10}\text{Be}$  minimum apparent exposure ages on two lateral moraines in the Turkestan Range (Aksu Valley), Kyrgyz Tian Shan, ranging from  $13.7 \pm 1.2$  to  $28.5 \pm 2.0$  ka ([Table 4](#), AK21 to AK25, and AK31 to AK35). [Koppes et al. \(2008\)](#) obtained a  $^{10}\text{Be}$  minimum apparent exposure age from the Ala Bash Basin ([Fig. 1](#)) of  $19.9 \pm 1.1$  ka ([Table 4](#)) and [Zech \(2012\)](#) obtained five  $^{10}\text{Be}$  minimum apparent exposure ages ranging from  $17.8 \pm 1.0$  to  $24.1 \pm 1.4$  ka from the Kitschi-Kurumdu Valley ([Fig. 1](#); all recalculated ages, [Table 4](#), KI21 to KI25). [Narama et al. \(2009\)](#) obtained five OSL ages from tills in four north-facing valleys in the At Bashi Range ([Fig. 1](#)) from 18 to 33 ka and [Narama et al. \(2007, 2009\)](#) also reported OSL ages from the Terskey Ala Tau Range from 21 to 29 ka.

Some studies have also suggested that there were Lateglacial events in the Tian Shan. For example, [Abramowski et al. \(2006\)](#) obtained three  $^{10}\text{Be}$  minimum apparent exposure ages from  $13.8 \pm 1.1$  to  $14.1 \pm 1.1$  ka ([Table 4](#), AV1 to AV3) on a moraine in the Koksu Valley of the Alay Range, Kyrgyz Tian Shan. [Zech \(2012\)](#) obtained four  $^{10}\text{Be}$  minimum apparent exposure ages on a moraine in the Kitschi-Kurumdu Valley from  $10.5 \pm 0.7$  to  $17.7 \pm 1.0$  ka, and suggested that they documented a Lateglacial advance (all recalculated ages; [Table 4](#), samples KI11 to KI14). In the eastern Tian Shan,  $^{10}\text{Be}$  minimum apparent exposure ages dated glacial events from 16 to 19 ka in the Daxi Valley ([Fig. 2](#), [Table 4](#)) that have been interpreted as evidence for Lateglacial advances ([Kong et al., 2009](#); [Li et al., 2011](#)). However, similar ages have not been found on the southern slope of the Tianger Range (Ala Valley).

In our study area of the eastern Tian Shan, no moraine ages record Holocene glacial events, except for the LIA, and this is similar to results from the western Tian Shan. [Koppes et al. \(2008\)](#) reported two  $^{10}\text{Be}$  exposure ages of  $0.32 \pm 0.08$  and  $0.69 \pm 0.12$  ka (recalculated, [Table 4](#)), indicating LIA glacial advances in the Ala Archa Valley in the Kyrgyz Front Range, Kyrgyz Tian Shan. Other than these two ages, few ages for glacial advances <10 ka have been reported in any studies in the Tian Shan. In the eastern Tian Shan,  $^{10}\text{Be}$  exposure ages just outside LIA moraines in the Daxi Valley are >16 ka ([Li et al., 2011](#), [Table 4](#), TS-07-23 and TS-07-25) and  $^{10}\text{Be}$  exposure ages from M1, 1.5 km downstream from LIA moraines in the Ala Valley, are >20 ka ([Table 2](#), [Fig. 5](#)). The lack of other Holocene deposits suggests limited glacial expansion during these phases and reworking of any deposits by more extensive expansion during the LIA.

In addition to cosmogenic nuclide and OSL techniques, ESR has been used to date glacial deposits in the Tian Shan ([Fig. 1](#); [Yi et al.,](#)

[2002](#); [Zhao et al., 2006, 2009, 2010, 2012](#)). However, the mechanisms by which an ESR signal is reset in glacial environments still remain unclear, and potential incomplete resetting of the ESR signal causes some concerns for the interpretation of ESR ages ([Kong et al., 2009](#); [Li et al., 2011](#); [Fu et al., 2013](#)). For example, in the Daxi Valley of the eastern Tian Shan, ESR dating of glacial deposits yielded ages that are far older than  $^{10}\text{Be}$  ages from the same landforms ([Kong et al., 2009](#); [Li et al., 2011](#)). ESR ages of 35–37 ka obtained by [Yi et al. \(2002\)](#) and [Zhao et al. \(2006\)](#) for the Upper Wangfeng moraine are roughly twice as old as the  $^{10}\text{Be}$  minimum apparent exposure ages of 17–19 ka obtained by [Li et al. \(2011\)](#) for the same moraine ([Table 4](#)). ESR ages from the Lower Wangfeng moraine/till of 54–73 ka obtained by [Yi et al. \(2002\)](#) and 171–184 ka obtained by [Zhao et al. \(2006\)](#) are three to ten times older than the  $^{10}\text{Be}$  minimum apparent exposure ages for this moraine of 18–21 ka ([Li et al., 2011](#); [Table 4](#), [Fig. 5](#)). In addition, significantly different ESR ages were obtained for the Lower Wangfeng moraine/till by the different investigators, although [Zhao et al. \(2006\)](#) proposed a solution to this by suggesting that this till may have been deposited in different stages and that the different ESR ages reflect different stages of deposition. However, additional detailed depositional evidence is needed to further evaluate this inference.

It is interesting to note that published ESR ages for glacial deposits in the Daxi Valley are somehow consistent with  $^{10}\text{Be}$  ages on moraines from the Ala Valley on the southern slope ([Fig. 5](#)). If the ESR ages are accurately dating glacial deposits, there is a possibility that they are recording the age of M3–M6 till beds overlain by surface material for which  $^{10}\text{Be}$  exposure ages record the last phase of glacial advance and/or retreat. These results illustrate that there remains a need for rigorous further testing to check the validity of using ESR to date glacial deposits.

## 5.2. Extent of Quaternary glaciations across the Tian Shan

The glacial event of MIS 6 or older (M6) is apparently the largest glaciation recorded in our study area in the eastern Tian Shan. During this period, glaciers from the Dundesala Valley and the Ala Valley merged. The interfluvial ridges were also likely covered by ice given the magnitude of the ELA depression at that time (>425 m) and the presence of erratics and till on the interfluvial ridges. The glacial event during MIS 4 (M5) was apparently more extensive than other glacial events during the Last Glaciation (MIS 5–MIS 2). Glaciers in the Ala Valley advanced at least 20 km down the valley and covered at least the lowest elevation sections of interfluvial ridges. However, evidence for the terminal position of this glacial event remains undetermined. The glacial event during MIS 3 (M4) remains well preserved in the Ala Valley and during this period glaciers advanced about 20 km down the valley and dammed tributaries on both sides of the main valley to form moraine-dammed lakes. The concomitant ELA depression that drove the glacier advance was about 425 m. During late MIS 3 to MIS 2 (M3 to M1), glaciers advanced about 10 km down the Ala Valley, corresponding to an ELA depression of approximately 225 m. The LIA is the only Holocene glacial event that can be identified in the Tianger Range, and is represented by two to three fresh-looking moraines flanking modern glacier margins and terminating a few hundred meters down-valley from modern glacier snouts. The ELA depression during the LIA glacial event of Glacier No. 1 in the Daxi Valley was about 50–80 m.

Whereas the Ala Valley includes glacial deposits dating to MIS 6 or older, 4, 3, and 2,  $^{10}\text{Be}$  ages in the Daxi Valley only represent glacial events during MIS 2 and 1 ([Kong et al., 2009](#); [Li et al., 2011](#); this paper). In addition,  $^{10}\text{Be}$  ages related to MIS 2 in the Daxi Valley (16–24 ka, [Table 4](#)) are ~6–9 ka younger than those of the Ala Valley (22–33 ka). This indicates that when glaciers in the Daxi

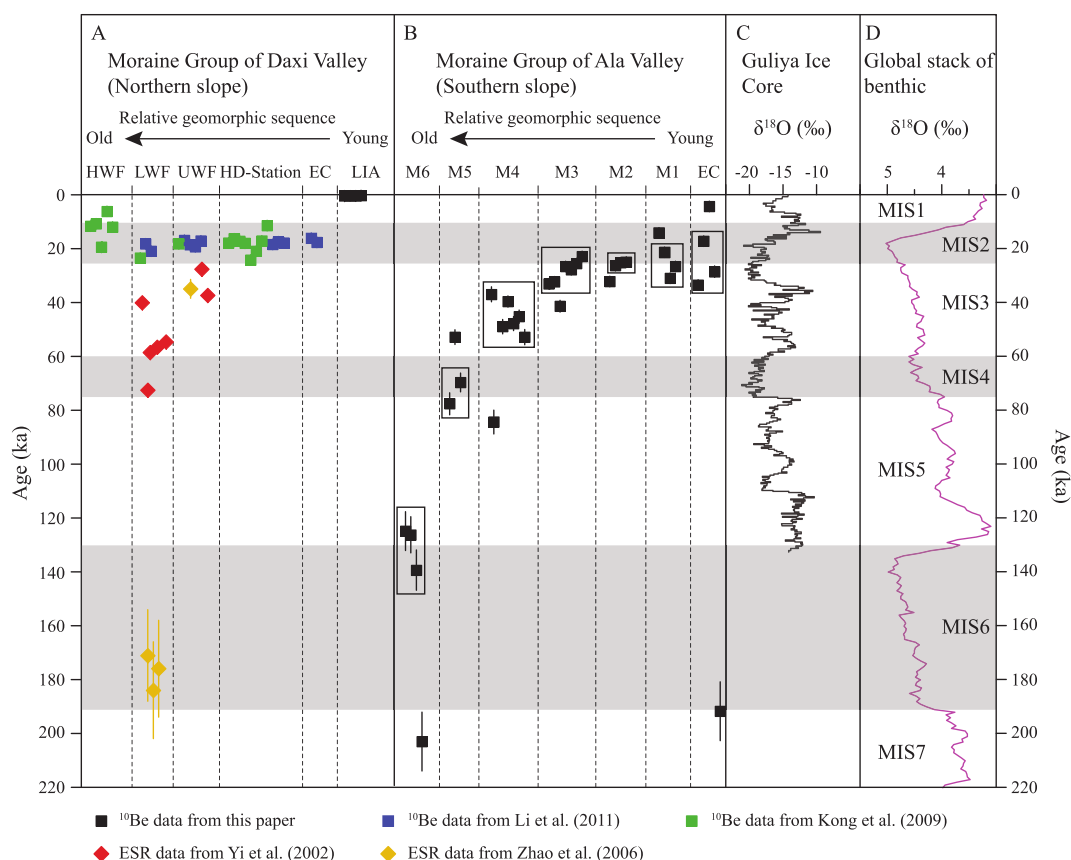


**Fig. 5.** Comparison of glacial chronologies constrained by  $^{10}\text{Be}$  surface exposure age dating from glacial deposits on the northern (A) and southern (B) slopes of the Tianger Range. The data are plotted against the  $\delta^{18}\text{O}$  record from the Guliya Ice Core from the northern Tibetan Plateau (C; Thompson et al., 1997;  $35^{\circ}17' \text{ N}$ ,  $81^{\circ}29' \text{ E}$ ) and the global stack of benthic  $\delta^{18}\text{O}$  records (D; Lisiecki and Raymo, 2005). ESR ages from the Daxi Valley (Yi et al., 2002; Zhao et al., 2006) are also illustrated in (A). UWF: Upper Wangfeng; LWF: Lower Wangfeng; HWF: Higher Wangfeng; HD-Station: Hayisa Drumlin to Tianshan Glaciological Station. Detailed description of these moraines and related glacial landforms can be found in Li et al. (2011).

Valley had advanced >10 km to attain their gLGM positions, glaciers in the Ala Valley had probably retreated to their M1 or M2 positions, and were therefore restricted to a position 2–5 km from the valley head. The age differences of the glacial events in these two valleys may be caused by differences in preservation and microclimate conditions. The northern slope of the Tianger Range (Daxi Valley) is relatively steep (Fig. 6A, B) with a relatively low hypsometric integral (HI) value ( $\text{HI} = 0.41$ , Fig. 6C), indicating that the valley has been relatively well dissected. Urumqi River has incised the Daxi Valley significantly up to 3200 m a.s.l. (Fig. 6A), where the most prominent glacial deposits are found. For example, bedrock is exposed in the river bed around the Wangfeng Station (3050 m a.s.l.; Fig. 2) where a >100 m high profile in the Lower Wangfeng till has become exposed (Zhao et al., 2006). Active headward erosion and slope instabilities caused by the relatively steep topography likely decrease the preservation potential of moraines; any moraine remnants from events older than MIS 2 in the Daxi Valley have thus apparently been eroded by fluvial erosion and post-glacial slope processes.

In contrast to the relatively steep, incised Daxi Valley, the Ala Valley has a relatively gentle gradient (Fig. 6A, B) with a relatively high HI value ( $\text{HI} = 0.54$ , Fig. 6C). River incision is only apparent up to 2900 m a.s.l., at the confluence between the Ala and Dundesala valleys (Fig. 2), leaving about 20 km of the upper Ala Valley and its source tributaries almost unaffected by rejuvenation. This situation favors the preservation of glacial landforms within the upper Ala Valley. Furthermore, the presence of a bedrock step at the

confluence of the Ala and Dundesala valleys also helps preserve evidence of older glacial events, although glacial deposits below this step have been eroded and so it is hard to reconstruct ELA depressions for the most extensive glaciations.

Additional to the difference in preservation conditions, these two valleys also face different aspects (Fig. 2). Modern glaciers mainly occur on northern slopes (such as the Daxi Valley) as these receive less direct solar radiation, which also favors other microclimatic conditions of preservation (for example, lower temperatures). It is possible that differences in aspect also have played an important role in the timing and extent of past glaciation, resulting in different glacial patterns in these two valleys.

Finally, we also examined the extent of different glacial events along the Tian Shan based on estimated ELA depressions ( $\Delta\text{ELA}$ , relative to the ELAs of modern glaciers) and the distances from the terminus of modern glaciers ( $\Delta\text{GL}$ ) in fifteen glacial valleys/sites, where glacial chronologies have been constrained using  $^{10}\text{Be}$  or OSL dating (Table 5, Fig. 7). The ELA depressions during MIS 4 varied greatly from 345 to 735 m along the Tian Shan and glaciers advanced between 7.8 and >20 km, except for an extreme high value of 51.6 km from the western Tian Shan/Pamirs (Abramowski et al., 2006, Fig. 7A). The ELA depressions during MIS 3 were around 400 m, except two extremely high values of 675 and 855 m from the western Tian Shan (Koppes et al., 2008). Corresponding glacier advances varied greatly, however, from 6.3 to 27.6 km (Fig. 7B), which is likely explained by differences in valley geometry and hypsometry. The ELA depressions during MIS 2 range from 160 to

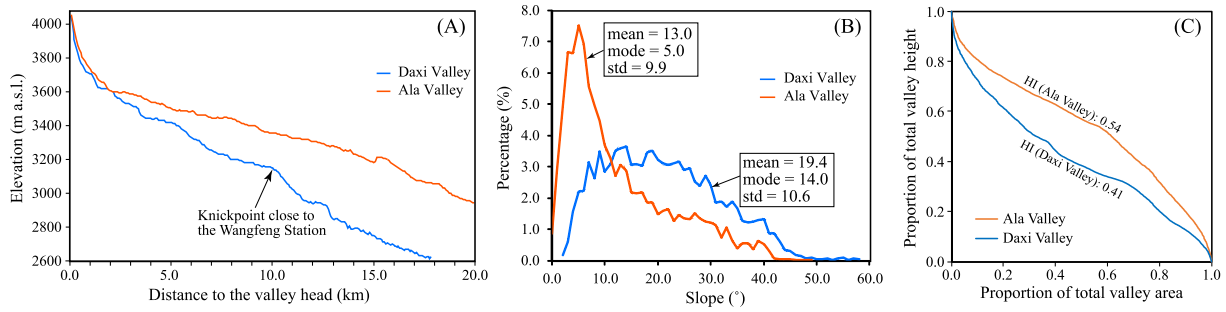


**Fig. 6.** Topographic characteristics of the Daxi and Ala valleys derived using the SRTM DEM. (A) Longitudinal topographic profiles (marked in Fig. 2). (B) Frequency distributions of slope gradients (°). (C) Hypsometric curves with their corresponding hypsometric integral (HI) values.

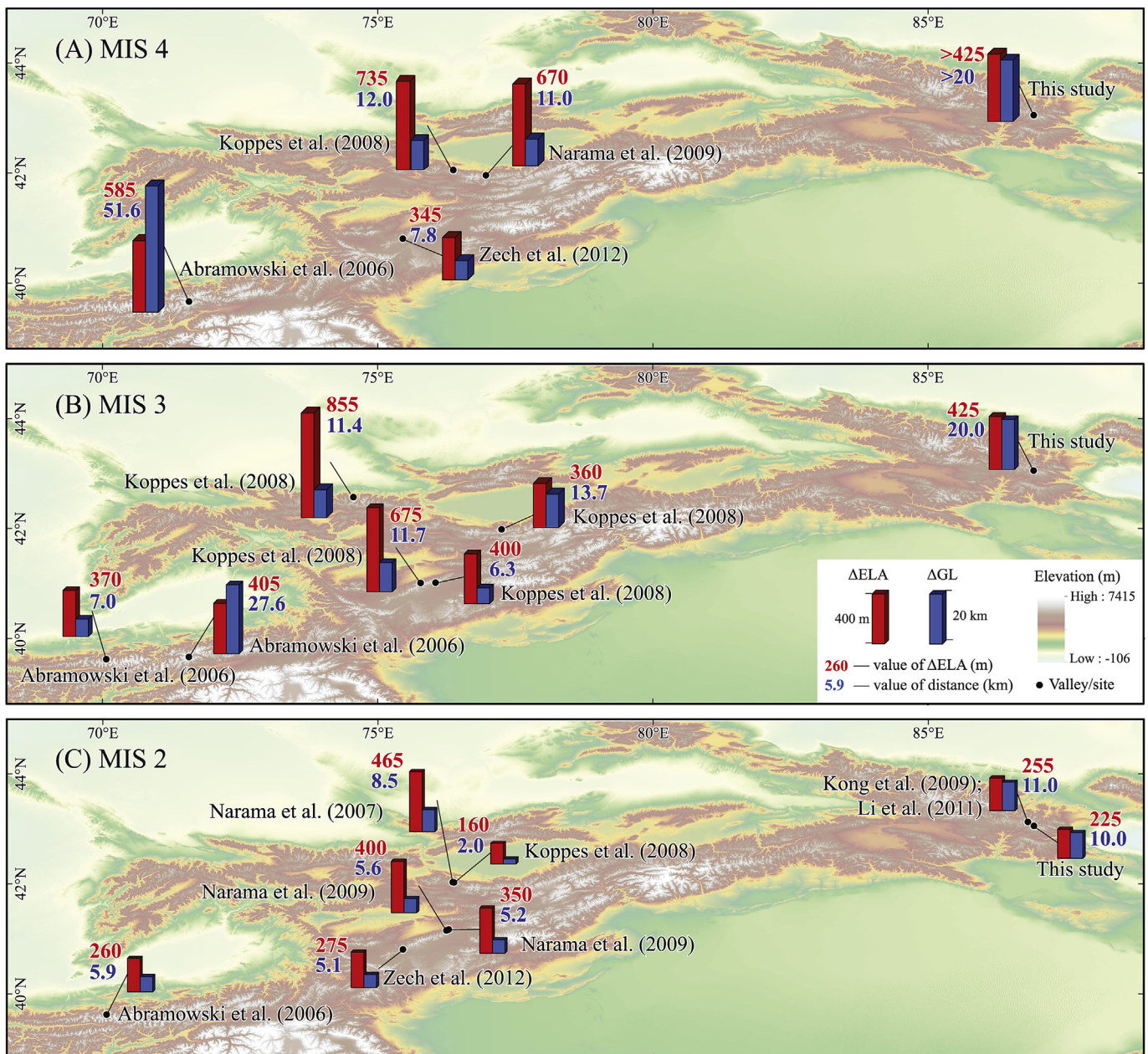


**Fig. 7.** ELA depressions ( $\Delta ELA$ ) and retreat distances ( $\Delta GL$ ) between glacial events during MIS 4 (A), MIS 3 (B), MIS 2 (C) and contemporary glaciation across the Tian Shan (Table 5).

**Table 5**  
Estimated changes in ELA ( $\Delta$ ELA in m) and glacier length ( $\Delta$ GL in km) during various glacial events across the Tian Shan.

Location	Valley/Site	Latitude ( $^{\circ}$ N)/ longitude ( $^{\circ}$ E)	Data source	MIS 6 or older		MIS 4		MIS 3		MIS 2		Lateglacial		LIA	
				$\Delta$ GL	$\Delta$ ELA	$\Delta$ GL	$\Delta$ ELA	$\Delta$ GL	$\Delta$ ELA	$\Delta$ GL	$\Delta$ ELA	$\Delta$ GL	$\Delta$ ELA	$\Delta$ GL	$\Delta$ ELA
Turkistan Range, Kyrgyzstan Alay Range, Kyrgyzstan Kyrgyz Front Range, Kyrgyzstan At Bashi Range, Kyrgyzstan	Aksu Valley	39.61/70.07	Abramowski et al. (2006)			51.6	585	7.0	370	5.9	260				
	Koksu Valley	39.65/71.57	Abramowski et al. (2006)					27.6	405			5.7	90		
	Ala Archa Valley	42.52/74.51	Koppes et al. (2008)					11.4	855					1.0	145
	Chor Kyrchak Valley	42.55/74.56	Koppes et al. (2008)					6.3	400						
	Djo Bog Gulsh Valley	41.00/76.05	Koppes et al. (2008)					11.7	675						
Terskey Ala Tau Range, Kyrgyzstan	Terekçu Valley	40.99/75.78	Narama et al. (2009)							5.6	400				
	Chong-Tör Valley	41.14/76.24	Zech et al. (2012)							<u>5.2</u>	<u>350</u>				
	Sary-Tal Valley	41.16/76.29								5.1	275				
	Kitschi-Kurumdu Valley	40.80/75.46	Koppes et al. (2008)					13.7	360			3.4	200		
Tianshan Range, China	Gulbel Pass	41.97/77.21	Narama et al. (2009)							2.0	160				
	Ala Bash Basin	42.01/76.38	Kong et al. (2009); Li et al. (2011); This paper	12.7	785	<u>11.0</u>	<u>670</u>								
	Temir-Kanat area	41.95/76.97								<u>8.5</u>	<u>465</u>				
	Turasu Valley	42.02/76.36								11.0	255				
	Daxi Valley	43.12/86.82								10.0	225				
	Ala Valley	43.04/86.93								>20	>425				
										>20	>425				

**Note:** Underlined number indicates the estimated value based on OSL ages.

465 m (from 160 to 275 m if only considering  $^{10}\text{Be}$  ages). Glacier advances during MIS 2 were mostly around 5–6 km in the western Tian Shan, whereas 10–11 km in the Daxi and Ala valleys in the eastern Tian Shan (Fig. 7C). In summary, we did not observe a clear west-east or a north-south pattern in ELA depressions for MIS 4–MIS 2 glacial events along and across the Tian Shan. The distances of glacier advances varied greatly across the Tian Shan, most likely reflecting the strong influence of local topography on glacial changes.

### 5.3. Paleoclimate implications

Glacier advances and retreats are controlled by temperature and precipitation. The timing of glaciation during MIS 6 or older is not dated with precision, which in turn inhibits useful comparisons with climate proxies. The evidence for MIS 4, 2, and 1 (LIA) glacial advances, on the other hand, correlates well with records of global temperature that show cold periods during these times (e.g., Clark et al., 1999; Fig. 5D). In contrast to northern hemisphere ice sheets, glacial events during the Last Glaciation in the Tian Shan became successively more restricted from MIS 4 to MIS 2. This pattern has been linked to arid conditions during the global LGM in the Central Asian highlands (e.g. Abramowski et al., 2006; Narama et al., 2007, 2009; Koppes et al., 2008). As the extent and height of the Fennoscandian Ice Sheet in Europe fluctuated between MIS 4 (smaller) and MIS 2 (peak) configurations, it would likely have been an orographic barrier that reduced the amount of moisture carried by the westerlies to Central Asia. This could explain that when the Fennoscandian Ice Sheet was less extensive, such as during the relatively mild MIS 4 period, more precipitation could be transported by the westerlies to Central Asian mountains, driving a more extensive MIS 4 glacier advance than MIS 2 advance.

Precipitation was perhaps also critically-responsible for driving significant glacier advances during MIS 3 in Central Asia, despite the fact that, globally, MIS 3 was a relatively warm period during the Last Glaciation (Fig. 5D). MIS 3 glacial events have been widely identified on the Tibetan Plateau and in Central Asian highlands (e.g. Phillips et al., 2000; Owen et al., 2005, 2009; Abramowski et al., 2006; Colgan et al., 2006; Koppes et al., 2008; Schäfer et al., 2008), and MIS 3 glacier advances in the Himalayas and on the southern Tibetan Plateau have been attributed to increased precipitation. Owen et al. (2002) suggested that increased solar radiation during MIS 3 strengthened the south Asian monsoon system and brought abundant precipitation to drive the inferred glacier advances (Owen et al., 2002). The Tian Shan is less affected by the south Asian monsoon, and MIS 3 glacier advances in this mountain range may instead be related to a strengthened westerlies circulation that brought more precipitation into this area. MIS 3 glacial events may also reflect a regional reduction in temperature (Shi et al., 2001; Wang, 2010). The Guliya ice core record from the northern Tibetan Plateau includes a relatively cold MIS 3 sub stage (MIS 3b, 54–44 ka; Fig. 5C) that might have contributed to triggering glacier advances in this region (Shi and Yao, 2002). MIS 3 glacial events constrained by  $^{10}\text{Be}$  exposure ages in the eastern and western Tian Shan are well correlated with the timing of this sub-stage.

Quaternary glaciations along and across the Tian Shan do not show an orographic effect, as there is no clear west-east or north-south pattern in ELA depressions for MIS 4, 3 and 2 glacier advances (Table 5, Fig. 7). Conditions that may counteract an expected orographic gradient in ELA depressions from west to east may relate to the Siberian High, which frequently delivers cold air masses to the eastern Tian Shan. The Siberian High was generally stronger over the past 400 years (across the LIA cooling period) than it has been for the past 25 years (Cong and Ho, 2002; D'Arrigo

et al., 2005). Hence, during colder periods than today, the Siberian High may have been strengthened and led to enhanced cold conditions in the eastern Tian Shan, resulting in an additional depression of the ELA relative to the western Tian Shan, perhaps counteracting the effect of limited precipitation.

## 6. Conclusions

Cosmogenic  $^{10}\text{Be}$  minimum apparent surface exposure ages for glacial landforms in the Daxi Valley and the Ala Valley, two major formerly-glaciated valleys in the Tianger Range, eastern Tian Shan, China, indicate that five major glacial events occurred in this region during MIS 6 or older, 4, 3, 2, and 1 (LIA). This glacial chronology is consistent with glacial chronologies from the western Tian Shan, indicating similar climate controls on the timing of Quaternary glaciations along this >1300 km section of the mountain range. However, only landforms and deposits from glacial events since MIS 2 are found on the northern slope in our study area of the eastern Tian Shan, whereas multiple events are recorded in landforms and deposits on the southern slope. This contrast may result from differences in landform preservation and micro-climatology due to differences in valley aspect and hypsometry. Glacier advances during the Last Glaciation (MIS 4, 3 and 2) became successively more restricted, probably reflecting the integrated effect of temperature and precipitation on glacier mass balance. LIA glacier advances are the only Holocene (MIS 1) glacial event recorded in the Tian Shan. Earlier Holocene glacier advances were either absent or extremely restricted so that they were destroyed by subsequent LIA glaciers.

An initial comparison between our  $^{10}\text{Be}$ -derived glacial chronology and published ESR ages for glacial deposits in the source area of Urumqi River indicates that these two methods are not producing consistent results. This may reflect problems with ESR resetting, or possibly that the sediment sampled for ESR dating was deposited by an earlier glaciation than that which deposited the surface material that was sampled for  $^{10}\text{Be}$ . If the latter is true, then this indicates a potential for using ESR dating to constrain the formation ages of glacial deposits, particularly where original surfaces have been destroyed by subsequent glacial or post-glacial erosion or have been covered by younger glacial or post-glacial sediments. Rigorous testing is still needed to check the validity of using ESR to date glacial deposits and the comparison with cosmogenic nuclide and OSL dating techniques may be beneficial.

## Acknowledgments

This work was supported by the National Natural Science Foundation of China (Grant Nos. 41328001, 40971002, 41101003, and 41230743). We acknowledge Lei Shi and Jingchun Zhang from Peking University for their help with field work, Chaolu Yi and Guocheng Dong from the Institute of Tibetan Plateau Research, Chinese Academy of Sciences, for sample preparation, and Tom Clifton and Susan Ma at PRIME Lab, Purdue University, for sample measurements and calculations. We thank two reviewers, Miriam Dühnforth and Delia Gheorghiu, for their constructive reviews.

## Appendix A. Supplementary data

Supplementary data related to this article can be found at <http://dx.doi.org/10.1016/j.quascirev.2014.05.009>.

## References

Abramowski, U., Bergau, A., Seebach, D., Zech, R., Glaser, B., Sosin, P., Kubik, P.W., Zech, W., 2006. Pleistocene glaciations of Central Asia: results from  $^{10}\text{Be}$  surface

- exposure ages of erratic boulders from the Pamir (Tajikistan), and the Alay–Turkistan range (Kyrgyzstan). *Quat. Sci. Rev.* 25, 1080–1096.
- Aizen, V.B., Aizen, E., Fujita, K., Nikitin, S.A., Kreutz, K.J., Takeuchi, L.N., 2005. Stable-isotope time series and precipitation origin from firn-core and snow samples, Altai glaciers, Siberia. *J. Glaciol.* 51, 637–654.
- Aizen, V.B., Aizen, E.M., Melack, J.M., Kreutz, K.J., Cecil, L.D., 2004. Association between atmospheric circulation patterns and firn-ice core records from the Inilchek glacierized area, central Tien Shan, Asia. *J. Geophys. Res. Atmos.* 109, D08304 <http://dx.doi.org/10.1029/2003JD003894>.
- Applegate, P.J., Urban, N.M., Laabs, B.J.C., Keller, K., Alley, R.B., 2010. Modeling the statistical distributions of cosmogenic exposure dates from moraines. *Geosci. Model Dev.* 3, 293–307.
- Balco, G., 2011. Contributions and unrealized potential contributions of cosmogenic-nuclide exposure dating to glacier chronology, 1990–2010. *Quat. Sci. Rev.* 30, 3–27.
- Balco, G., Briner, J., Finkel, R.C., Rayburn, J.A., Ridge, J.C., Schäfer, J.M., 2009. Regional beryllium-10 production rate calibration for northeastern North America. *Quat. Geochronol.* 4, 93–107.
- Balco, G., Stone, J.O., Lifton, N.A., Dunai, T.J., 2008. A complete and easily accessible means of calculating surface exposure ages or erosion rates from  $^{10}\text{Be}$  and  $^{26}\text{Al}$  measurements. *Quat. Geochronol.* 3, 174–195.
- Benn, D.I., Lehmkuhl, F., 2000. Mass balance and equilibrium-line altitudes of glaciers in high-mountain environments. *Quat. Int.* 65–6, 15–29.
- Benn, D.I., Owen, L.A., 1998. The role of the Indian summer monsoon and the mid-latitude westerlies in Himalayan glaciation: review and speculative discussion. *J. Geol. Soc.* 155, 353–363.
- Briner, J.P., 2009. Moraine pebbles and boulders yield indistinguishable Be-10 ages: a case study from Colorado, USA. *Quat. Geochronol.* 4, 299–305.
- Briner, J.P., Kaufman, D.S., Manley, W.F., Finkel, R.C., Caffee, M.W., 2005. Cosmogenic exposure dating of late Pleistocene moraine stabilization in Alaska. *Geol. Soc. Am. Bull.* 117, 1108–1120.
- Chen, J., 1989. Preliminary researches on lichenometric chronology of Holocene glacial fluctuations and on other topics in the headwater of Urumqi River, Tianshan Mountains. *Sci. China (Ser. B)* 32, 1487–1500 (in Chinese).
- Clark, P.U., Alley, R.B., Pollard, D., 1999. Northern hemisphere ice-sheet influences on global climate change. *Science* 286, 1104–1111.
- Clark, P.U., Dyke, A.S., Shakun, J.D., Carlson, A.E., Clark, J., Wohlfarth, B., Mitrovica, J.X., Hostetler, S.W., McCabe, A.M., 2009. The last glacial maximum. *Science* 325, 710–714.
- Colgan, P.M., Munroe, J.S., Zhou, S., 2006. Cosmogenic radionuclide evidence for the limited extent of last glacial maximum glaciers in the Tanggula Shan of the central Tibetan Plateau. *Quat. Res.* 65, 336–339.
- Cui, Z., 1981. Glacial erosion landforms and development of trough at the head of Urumqi River, Tian Shan. *J. Glaciol. Geocryol.* 3, 1–15 (in Chinese).
- D'Arrigo, R., Jacoby, G., Wilson, R., Panagiotopoulos, F., 2005. A reconstructed Siberian High index since A.D. 1599 from Eurasian and North American tree rings. *Geophys. Res. Lett.* 32, L05705 <http://dx.doi.org/10.1029/2004GL022271>.
- Desilets, D., Zreda, M., 2003. Spatial and temporal distribution of secondary cosmic-ray neutron intensities and applications to in situ cosmogenic dating. *Earth Planet. Sci. Lett.* 206, 21–42.
- Desilets, D., Zreda, M., Prabu, T., 2006. Extended scaling factors for in situ cosmogenic nuclides: new measurements at low latitude. *Earth Planet. Sci. Lett.* 246, 265–276.
- Dunai, T., 2001. Influence of secular variation of the magnetic field on production rates of in situ produced cosmogenic nuclides. *Earth Planet. Sci. Lett.* 193, 197–212.
- Ehlers, J., Gibbard, P.L., 2007. The extent and chronology of cenozoic global glaciation. *Quat. Int.* 164–166, 6–20.
- Fabel, D., Harbor, J., Dahms, D., James, A., Elmore, D., Horn, L., Daley, K., Steele, C., 2004. Spatial patterns of glacial erosion at a valley scale derived from terrestrial cosmogenic Be-10 and Al-26 concentrations in rock. *Ann. Assoc. Am. Geogr.* 94, 241–255.
- Fu, P., Stroeven, A.P., Harbor, J.M., Hättestrand, C., Heyman, J., Caffee, M.W., Zhou, L.P., 2013. Paleoglaciation of Shaluli Shan, Southeastern Tibetan Plateau. *Quat. Sci. Rev.* 64, 121–135.
- Gong, D.Y., Ho, C.H., 2002. The Siberian High and climate change over middle to high latitude Asia. *Theor. Appl. Climatol.* 72, 1–9.
- Hallet, B., Putkonen, J., 1994. Surface dating of dynamic landforms: young boulders on aging moraines. *Science* 265, 937–940.
- Henderson, K., Laube, A., Gaggeler, H.W., Olivier, S., Papina, T., Schwikowski, M., 2006. Temporal variations of accumulation and temperature during the past two centuries from Belukha ice core, Siberian Altai. *J. Geophys. Res. Atmos.* 111, D03104 <http://dx.doi.org/10.1029/2005JD005819>.
- Heyman, J., Stroeven, A.P., Caffee, M.W., Hättestrand, C., Harbor, J., Li, Y.K., Alexanderson, H., Zhou, L.P., Hubbard, A., 2011a. Palaeoglaciology of Bayan Har Shan, NE Tibetan Plateau: exposure ages reveal a missing LGM expansion. *Quat. Sci. Rev.* 30, 1988–2001.
- Heyman, J., Stroeven, A.P., Harbor, J., Caffee, M.W., 2011b. Too young or too old: evaluating cosmogenic exposure dating based on an analysis of compiled boulder exposure ages. *Earth Planet. Sci. Lett.* 302, 71–80.
- Kaplan, M.R., Strelin, J.A., Schäfer, J.M., Denton, G.H., Finkel, R.C., Schwartz, R., Putnam, A.E., Vandergoes, M.J., Goehring, B.M., Travis, S.G., 2011. In-situ cosmogenic Be-10 production rate at Lago Argentino, Patagonia: implications for late-glacial climate chronology. *Earth Planet. Sci. Lett.* 309, 21–32.

- Kohl, C.P., Nishiizumi, K., 1992. Chemical isolation of quartz for measurement of in situ -produced cosmogenic nuclides. *Geochim. Cosmochim. Acta* 56, 3583–3587.
- Kong, P., Fink, D., Na, C., Huang, F., 2009. Late Quaternary glaciation of the Tianshan, Central Asia, using cosmogenic  $^{10}\text{Be}$  surface exposure dating. *Quat. Res.* 72, 229–233.
- Koppes, M., Gillespie, A.R., Burke, R.M., Thompson, S.C., Stone, J., 2008. Late Quaternary glaciation in the Kyrgyz Tien Shan. *Quat. Sci. Rev.* 27, 846–866.
- Kreutz, K.J., Aizen, V.B., Cecil, L.D., Wake, C.P., 2001. Oxygen isotopic and soluble ionic composition of a shallow firn core, Inilchek Glacier, central Tien Shan. *J. Glaciol.* 47, 548–554.
- Lal, D., 1991. Cosmic ray labeling of erosion surfaces: in situ nuclide production rates and erosion models. *Earth Planet. Sci. Lett.* 104, 424–439.
- Li, S., 1995. Ancient environment reconstruction in the late Pleistocene at the head of Urumqi Valley, Tianshan. In: Li, J.J., Wu, Z., Xu, S.Y., et al. (Eds.), *Geomorphology-Environment-Development*. Environmental Science Press of China, Beijing, pp. 14–18 (in Chinese).
- Li, Y.K., 2013. Determining topographic shielding from digital elevation models for cosmogenic nuclide analysis: a GIS approach and field validation. *J. Mt. Sci.* 10, 355–362.
- Li, Y.K., Harbor, J., Stroeven, A.P., Fabel, D., Kleman, J., Fink, D., Caffee, M., Elmore, D., 2005. Ice sheet erosion patterns in valley systems in northern Sweden investigated using cosmogenic nuclides. *Earth Surf. Process. Landf.* 30, 1039–1049.
- Li, Y.K., Liu, G.N., Cui, Z.J., 2001a. Glacial valley cross-profile morphology, Tian Shan Mountains, China. *Geomorphology* 38, 153–166.
- Li, Y.K., Liu, G.N., Cui, Z.J., 2001b. Longitudinal variations in cross-section morphology along a glacial valley: a case-study from the Tien Shan, China. *J. Glaciol.* 47, 243–250.
- Li, Y.K., Liu, G.N., Kong, P., Harbor, J., Chen, Y.X., Caffee, M., 2011. Cosmogenic nuclide constraints on glacial chronology in the source area of the Urumqi River, Tian Shan, China. *J. Quat. Sci.* 26, 297–304.
- Lifton, N., Bieber, J., Clem, J., Duldig, M., Evenson, P., Humble, J., Pyle, R., 2005. Addressing solar modulation and long-term uncertainties in scaling secondary cosmic rays for in situ cosmogenic nuclide applications. *Earth Planet. Sci. Lett.* 239, 140–161.
- Lisiecki, L.E., Raymo, M.E., 2005. A Pliocene-Pleistocene stack of 57 globally distributed benthic  $\delta^{18}\text{O}$  records. *Paleoceanography* 20, PA1003. <http://dx.doi.org/10.1029/2004PA001071>.
- Maisch, M., 1992. Die Gletscher Graubündens: Rekonstruktionen und Auswertung der Gletscher und deren Veränderungen seit dem Hochstand von 1850 im Gebiet der östlichen Schweizer Alpen (Bündnerland und angrenzende Regionen). In: *Physische Geographie*, vol. 33. Universität Zürich, Zürich.
- Narama, C., Kondo, R., Tsukamoto, S., Kajiura, T., Duishonakunov, M., Abdrakhmatov, K., 2009. Timing of glacier expansion during the Last Glacial in the inner Tien Shan, Kyrgyz Republic by OSL dating. *Quat. Int.* 199, 147–156.
- Narama, C., Kondo, R., Tsukamoto, S., Kajiura, T., Ormukov, C., Abdrakhmatov, K., 2007. OSL dating of glacial deposits during the Last Glacial in the Terskey-Alatau Range, Kyrgyz Republic. *Quat. Geochronol.* 2, 249–254.
- Nie, Z.Y., Pan, R.Y., Li, C.C., Zhang, M., Liu, G.N., 2014. Analysis of the glacial geomorphological characteristics of the last glacial in the Tianger area, Tien Shan, and their paleoclimate implications. *Ann. Glaciol.* 55 (66), 52–60.
- Nishiizumi, K., Imamura, M., Caffee, M.W., Southon, J.R., Finkel, R.C., McAninch, J., 2007. Absolute calibration of  $^{10}\text{Be}$  AMS standards. *Nucl. Instrum. Methods Phys. Res. Sect. B Beam Interact. Mater. Atoms* 258, 403–413.
- Olivier, S., Schwikowski, M., Brutsch, S., Eyrikh, S., Gaggeler, H.W., Luthi, M., Papina, T., Saurer, M., Schotterer, U., Tobler, L., Vogel, E., 2003. Glaciochemical investigation of an ice core from Belukha glacier, Siberian Altai. *Geophys. Res. Lett.* 30 (2019), 19 <http://dx.doi.org/10.1029/2003GL018290>.
- Owen, L.A., Finkel, R.C., Barnard, P.L., Ma, H., Asahi, K., Caffee, M.W., Derbyshire, E., 2005. Climatic and topographic controls on the style and timing of Late Quaternary glaciation throughout Tibet and the Himalaya defined by  $^{10}\text{Be}$  cosmogenic radionuclide surface exposure dating. *Quat. Sci. Rev.* 24, 1391–1411.
- Owen, L.A., Finkel, R.C., Caffee, M.W., 2002. A note on the extent of glaciation throughout the Himalaya during the global Last Glacial Maximum. *Quat. Sci. Rev.* 21, 147–157.
- Owen, L.A., Robinson, R., Benn, D.I., Finkel, R.C., Davis, N.K., Yi, C., Putkonen, J., Li, D., Murray, A.S., 2009. Quaternary glaciation of Mount Everest. *Quat. Sci. Rev.* 28, 1412–1433.
- Phillips, W.M., Sloan, V.F., Shroder, J.F., Sharma, P., Clarke, M.L., Rendell, H.M., 2000. Asynchronous glaciation at Nanga Parbat, northwestern Himalaya Mountains, Pakistan. *Geology* 28, 431–434.
- Putkonen, J., Swanson, T., 2003. Accuracy of cosmogenic ages for moraines. *Quat. Res.* 59, 255–261.
- Putnam, A.E., Schäfer, J.M., Barrell, D.J.A., Vandergoes, M., Denton, G.H., Kaplan, M.R., Finkel, R.C., Schwartz, R., Goehring, B.M., Kelley, S.E., 2010. In situ cosmogenic Be-10 production-rate calibration from the Southern Alps, New Zealand. *Quat. Geochronol.* 5, 392–409.
- Röhringer, I., Zech, R., Abramowski, U., Sosin, P., Aldahan, A., Kubik, P.W., Zoller, L., Zech, W., 2012. The late Pleistocene glaciation in the Bogchigir Valleys (Pamir, Tajikistan) based on Be-10 surface exposure dating. *Quat. Res.* 78, 590–597.
- Schäfer, J.M., Oberholzer, P., Zhao, Z., Ivy-Ochs, S., Wieler, R., Baur, H., Kubik, P.W., Schlüchter, C., 2008. Cosmogenic beryllium-10 and neon-21 dating of late Pleistocene glaciations in Nyalam, monsoonal Himalayas. *Quat. Sci. Rev.* 27, 295–311.
- Seong, Y.B., Owen, L.A., Bishop, M.P., Bush, A., Clendon, P., Copland, L., Finkel, R., Kamp, U., Shroder, J.F., 2007. Quaternary glacial history of the Central Karakoram. *Quat. Sci. Rev.* 26, 3384–3405.
- Shi, Y., Yao, T., 2002. MIS3b (54–44 ka BP) cold period and glacial advance in middle and low latitudes. *J. Glaciol. Geocryol.* 24, 1–9 (in Chinese).
- Shi, Y., Yu, G., Liu, X., Li, B., Yao, T., 2001. Reconstruction of the 30–40 ka BP enhanced Indian monsoon climate based on geological records from the Tibetan Plateau. *Palaeogeogr. Palaeoclimatol. Palaeoecol.* 169, 69–83.
- Sorg, A., Bolch, T., Stoffel, M., Solomina, O., Beniston, M., 2012. Climate change impacts on glaciers and runoff in Tien Shan (Central Asia). *Nat. Clim. Change* 2, 725–731.
- Stone, J.O., 2000. Air pressure and cosmogenic isotope production. *J. Geophys. Res. Solid Earth* 105, 23753–23759.
- Stroeven, A.P., Fabel, D., Hättestrand, C., Harbor, J., 2002. A relict landscape in the centre of Fennoscandian glaciation: cosmogenic radionuclide evidence of tors preserved through multiple glacial cycles. *Geomorphology* 44, 145–154.
- Stroeven, A.P., Hättestrand, C., Heyman, J., Kleman, J., Morén, B.M., 2013. Glacial geomorphology of the Tien Shan. *J. Maps* 9 (4), 505–512.
- Thackray, G.D., Owen, L.A., Yi, C.L., 2008. Timing and nature of late Quaternary mountain glaciation. *J. Quat. Sci.* 23, 503–508.
- Thompson, L.G., Yao, T., Davis, M.E., Henderson, K.A., Mosley-Thompson, E., Lin, P.N., Beer, J., Synal, H.A., Cole-Dai, J., Bolzan, J.F., 1997. Tropical climate instability: the last glacial cycle from a Qinghai-Tibetan ice core. *Science* 276, 1821–1825.
- Wang, J., 1981. Ancient glaciers at the head of Urumqi River, Tian Shan. *J. Glaciol. Geocryol.* 3, 55–63 (in Chinese).
- Wang, J., 2010. Glacial advance in the Qinghai-Tibet Plateau and peripheral mountains during the mid-MIS 3. *Quat. Sci.* 30, 1055–1065 (in Chinese).
- Yi, C., Jiao, K., Liu, K., He, Y., Ye, Y., 2002. ESR dating of the sediments of the Last Glaciation at the source area of the Urumqi River, Tian Shan Mountains, China. *Quat. Int.* 97–8, 141–146.
- Yi, C.L., Liu, K.X., Cui, Z.J., Jiao, K.Q., Yao, T.D., He, Y.Q., 2004. AMS radiocarbon dating of late Quaternary glacial landforms, source of the Urumqi River, Tien Shan - a pilot study of C-14 dating on inorganic carbon. *Quat. Int.* 121, 99–107.
- Zech, R., 2012. A late Pleistocene glacial chronology from the Kitschi-Kurumdu Valley, Tien Shan (Kyrgyzstan), based on Be-10 surface exposure dating. *Quat. Res.* 77, 281–288.
- Zech, R., Röhringer, I., Sosin, P., Kabgov, H., Merchel, S., Akhmadaliev, S., Zech, W., 2013. Late Pleistocene glaciations in the Gissar Range, Tajikistan, based on  $^{10}\text{Be}$  surface exposure dating. *Palaeogeogr. Palaeoclimatol. Palaeoecol.* 369, 253–261.
- Zhao, J., Lai, Z., Liu, S., Song, Y., Li, Z., Yin, X., 2012. OSL and ESR dating of glacial deposits and its implications for glacial landform evolution in the Bogeda Peak area, Tianshan range, China. *Quat. Geochronol.* 10, 237–243.
- Zhao, J., Liu, S., He, Y., Song, Y., 2009. Quaternary glacial chronology of the Ateaoyinake River Valley, Tianshan Mountains, China. *Geomorphology* 103, 276–284.
- Zhao, J., Song, Y., King, J.W., Liu, S., Wang, J., Wu, M., 2010. Glacial geomorphology and glacial history of the Muzart River valley, Tianshan Range, China. *Quat. Sci. Rev.* 29, 1453–1463.
- Zhao, J., Zhou, S., He, Y., Ye, Y., Liu, S., 2006. ESR dating of glacial tills and glaciations in the Urumqi River headwaters, Tianshan Mountains, China. *Quat. Int.* 144, 61–67.
- Zheng, B., Zhang, Z., 1983. Fluctuation of glaciers during Neoglaciation in Bogda and the Urumqi River head, Tianshan. *J. Glaciol. Geocryol.* 5, 133–142 (in Chinese).